Electrochemical protein detection by target-responsive programmable dynamic DNA assembly

Electrochemical protein detection by target-responsive programmable dynamic DNA assembly

By Md Roqibul Hasan, M. Sc.

A Thesis Submitted to the School of Graduate Studies in the Partial Fulfillment of the Requirements for the Degree Masters of Applied Science.

McMaster University MASTERS OF APPLIED SCIENCE (2017) Hamilton, Ontario (Biomedical Engineering)

TITLE: Electrochemical protein detection by target-responsive programmable dynamic DNA assembly

AUTHOR: Md Roqibul Hasan,

SUPERVISOR: Dr. Leyla Soleymani

NUMBER OF PAGES: xii, 93

Abstract

Nucleic acid amplification is responsible for pushing the limit-of-detection of molecular diagnostic assays to unprecedented levels. We developed an assay based on protein-responsive programmable dynamic DNA assembly (PRPDA) to detect proteins via an intermediate process involving nucleic acids for taking advantage of nucleic acid amplification strategies. PRPDA has previously been designed for sensitive protein analysis in fluorescent assay formats [1]. To further push the detection limit and to achieve assay miniaturization and multiplexing, we sought to combine PRPDA with electrochemical readout. We were able to achieve LOD of 1 pM by employing wrinkled gold electrode for the PRDA protein detection scheme. Which is 2800 times improvement compare to the 2.8 nM demonstrated by fluorescent transduction [1].

Acknowledgements

First, I would like to thank my supervisor, Dr. Leyla Soleymani. I am indebted to her for accepting me into the group when I had very little experience in the field of electrochemistry. I learned a lot about research. I benefited greatly from her vision and creativity, and I was very lucky to be in such an exciting intellectual environment.

Within the lab, there are several members who acted as mentors and as good friends. Barnabas Fung was one of the first members that I learned a lot from, who was always available for extensive discussions. I have had the privilege to work alongside and become friends with the team, including Amin Hosseini, Jie Yang, Christine Gabardo, Sudip Saha, Larona Toteng, Eric Daigle, Yuting Chan, Amanda Victorious, Sadman Sakib, Marta Skreta. You were always there whenever needed, thank you.

I would also like to thank my collaborators, Dr. Feng Li and Alex Wang. The idea of this project stems from Dr. Li. Thanks, Dr. Li for always be available to provide your valuable insight whenever I was stuck during the project. Thanks Alex for helping me to establish project at the very initial stage.

I don't think I can acknowledge all the people whose friendship was valuable during my studies: Dr. Zia Khan, Dewan Ferdewas Wahid, Nazmul Hasan, Omar Sharif, I can't thank you enough for always be there for me as a friend and family far away from home.

Finally, I would like to acknowledge my family. I would like to express my deepest gratitude to my parents Ashab Uddin and Nasima Shehnaz, my sister Maliha for always being there to uplift me when I was going through an emotionally distressing stage. Thank you for the unconditional love you always have shown me. All the support they have provided me over the years was the greatest gift anyone has ever given me.

Contents

List of Figures

List of Tables

Acronyms

ACV Alternate Current Voltammetry

CE Counter Electrode

CV Cyclic Voltammetry

DPV Differential pulse voltammetry

LOD Limit of Detection

POC Point of Care

RE Reference Electrode

SWV Square Wave Voltammetry

WE Working Electrode

Declaration of Authorship

I, Md Roqibul Hasan, hereby declare that I am the sole author of this thesis titled, "Electrochemical protein detection by target-responsive programmable dynamic DNA assembly". This is a true copy of the thesis, including any required final revisions, as accepted by my examiners.

I understand that my thesis may be made electronically available to the public.

Chapter 1

Introduction

Discovery of increasing number of genes and mutations responsible for causing diseases [2] gave urgency for developing simple, cost-effective and easy-to-use tools to detect these identified mutations for diseases diagnostic. Point of Care (POC) detection of the diseases is critical for the detection of life-threatening diseases like cancer at the early stage.

1.1 Background on Biosensors

Biosensors were first demonstrated in the 1960s by the pioneers Clark and Lyons [3]. The term "Biosensor" was coined by Dr. Cammann [4], and its widely accepted definition was introduced by the International Union of Pure and Applied Chemistry (IUPAC) [5, 6]. According to IUPAC: *"Biosensor is a self-contained integrated device, which is capable of providing specific quantitative or semi-quantitative analytical information using a biological recognition element which is retained in direct spatial contact with a transducer element."* [6]. High specificity, independent of physical parameters such as pH and temperature and re-usability are the quintessential parameters of a biosensor [3].

As illustrated in Figure 1.1, the major components of the biosensors have two parts, the molecular recognition materials, and the signal transducer, where the interaction of the recognizing materials with the sample target analyte latter converts into the read-out data. Hence, the selectivity and the sensitivity of the biosensors are determined by the bio-recognition element and the transducer respectively. Bio-recognizing materials or named "probe" could be either affinity-based, such as nucleic acids (DNA/RNA/PNA), antibodies or biocatalytic such as enzyme, microorganisms or tissue materials [7]. Mostly used signal transduction includes electrochemical, optical or mass based detectors.

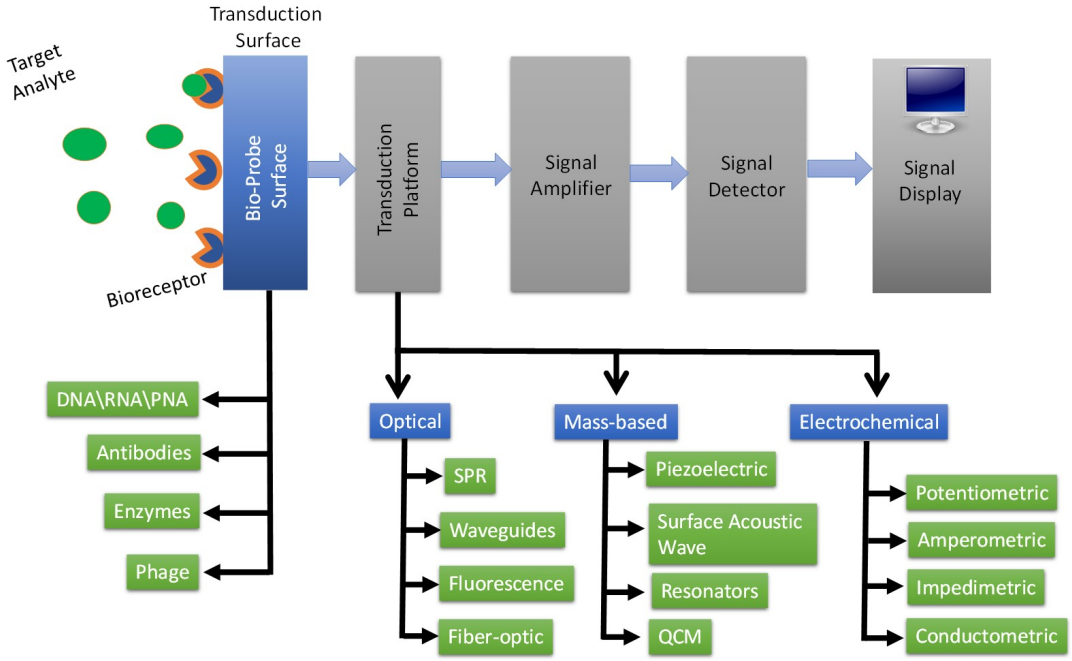

Figure 1.1: Major components of biosensors, including a bio-recognition element composed of bioreceptors and a transducer mechanism followed by Signal Amplification and Display setting. Adapted from reference [8] with the permission from the Royal Society of Chemistry.

Electrochemical readout provides significant advantages over the widely used optical readout such as fluorescent based techniques [9–11]. Some of the major advantages of

the biosensors developed based on electrochemical transduction that includes; simple to design electrodes that have the flexibility of miniaturization, the possibility of real-time detection with consecutive measurement of a different sample with a stable sensor response and detection platform amenable to the point of care system etc. [11]. Portability provides an electrochemical sensor to use at the point of care sites. Ease of miniaturization and multiplexing provide electrochemical biosensor the tunability to push the limit of detection of the sensor to an unprecedented level.

Figure 1.2: A) The EmStat USB powered potentiostats (Smallest electrochemical interfaces available on the market). B) PalmSense3 is USB and battery-powered handheld potentiostat and impedance analyzer which allows the application of most of the relevant voltammetric and amperometric techniques. C) Electrochemical sensor platform (electrodes) that are prepared on the flexible and easy to prepare substrates. Adapted from palmsense website [12].

1.2 Signal Transduction

As shown in Figure 1.1, bimolecular sensors widely employ optical, electrochemical and mass-based transduction techniques to convert the bioanalytical interaction with the detection assay in a readable format. The proposed protein detection model for this thesis was previously demonstrated with fluorescence transduction strategy, and we proposed to develop a similar assay using electrochemical transduction, a short literature review

on fluorescence-based and electrochemical-based transduction techniques discussed in this section.

1.2.1 Fluorescence transduction

A Fluorescence biosensor employs fluorescent tag to determine optical change before and after target interact with the capture molecule. Figure 1.3 shows main types fluorescent labeling for the DNA hybridization detection found in the literature. A direct labeling strategy can be employed where the immobilized DNA probe hybridizes with the labeled DNA target (Figure 1.3, left, b). A sandwich type complex can also be formed, where immobilized DNA probe hybridizes to a part of the target whereas the other of the target is complementary to a signaling DNA sequence that serves to label the target upon hybridization [13]. Molecular beacons (MB) can be used to detect DNA by fluorescence readout (Figure 1.3 right). MBs are single-stranded oligodeoxynucleotides (ODN) probes that possess a stem-and-loop structure. The loop portion is complementary to the target (Figure 1.3 right, top). A fluorophore and a sequence are linked to the two ends of the stem. In its native state, the probe is hairpin, and the two ends of the MB are nearby. The fluorescence of the fluorophore is quenched by energy transfer. Their hairpin stem is less stable than the binding between the loop and the target. In the presence of the target, the MB undergoes a conformational reorganization because the loop hybridizes with the target. The structure is opened, separating the fluorophore and the sequence. In this case, the MB emits an intense fluorescence signal [14–18].

A very early work demonstrated based on Fluorescence transduction achieved by Krull et al. shows the possibility to detect DNA hybridization with ssDNA (Single-Stranded DNA) probe immobilized on the surface of the quartz optical fibers, where they used Ethidium Bromide fluorescence tag as a reporter [19]. After hybridization to the probe, fluorescence signals were generated with ethidium bromide, which correlated

quantitatively with the level of bound DNA target. This nucleic acid assay has a detection limit of 86 nM [20]. The assays developed by Abel et al. with the similar concept as krull et al. demonstrated 10^5 times increased detection limits for labeled targets and 10^2 times improved for unlabeled DNA target detection limits compared to the reported by krull et al. [21].

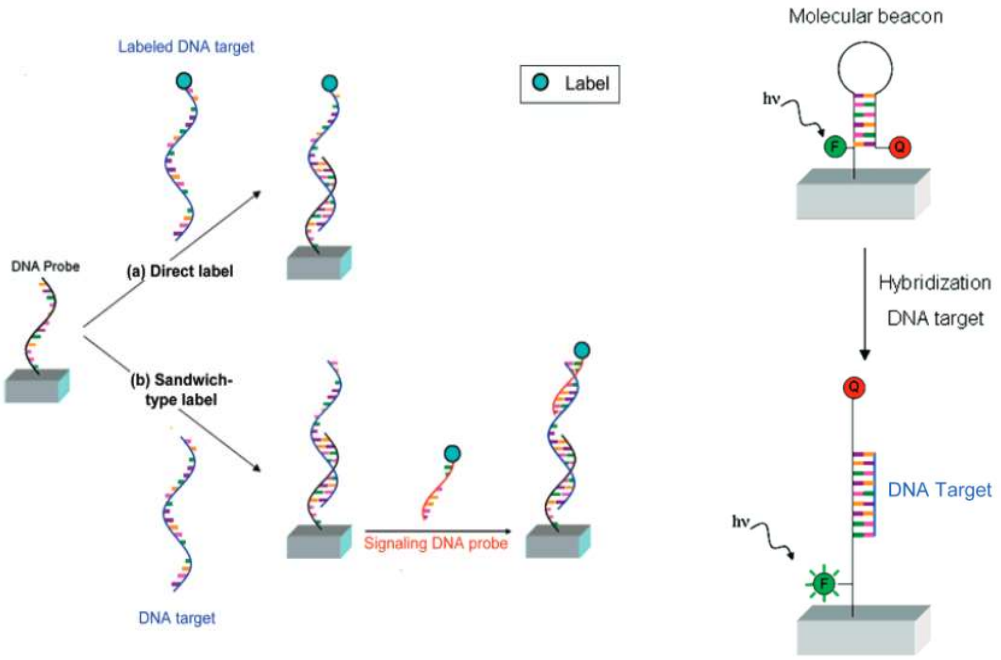

Figure 1.3: (left) Main types of labeled Flurosence based DNA biosensors and micro arrays a) direct label between immobilized DNA probe and labledled DNA target b) sandwithc-tupe system. A sandwich-type tenary complex is formed between immobilized DNA probe, target and signaling DNA probe. (Right) A DNA biosensor based on molecular beacon principle. Adapted from reference [22] with the permission from the ACS Publications

1.2.2 Electrochemical Transduction

High sensitivity and selectivity, compatibility with microfabrication and comparatively low fabrication cost, and miniaturization capability of the electrochemical readout urged the scientific community to widely employ this method in the biosensing field [23–27]. Biosensors utilizing electrochemical readout can be categorized into four classes; potentiometric, impedimetric, amperometric & voltammetric. Potentiometric devices measure the charge or potential collected at a sensor surface with respect to a reference when no current flows and provides information on ion activity. Impedimetric device measure impedance change; resistance/or capacitance at the sensor surface. The term amperometry describes the technique in which a fixed potential measured with respect to a reference electrode is applied to a working electrode and the current resulting from oxidation or reduction reactions occurring at the working electrode is measured. The voltammetric technique was used in this thesis, where a changing potential applied to the working electrode with respect to a reference and the current resulting from the reaction of analyzed species at the working electrode is recorded. The key factor in voltammetry is that the applied potential is varied over the course of the measurement. Most voltammetric electrochemical biosensors are three electrode systems comprised of a working (WE), counter (CE) and a reference (RE) electrode. Electrochemical reactions usually take places in the vicinity of the WE's. Details of a typical three-electrode system discussed in the next chapter.

Electrochemical methods are well established for DNA detection. Umek et al. (2001) were able to detect up to 50 nM nucleic acid target concentration with AC voltammetry utilizing the approach with a three-component sandwich assay [28]. In their assay, the redox label was attached to synthetic sequence specifically designed to bind an overhang portion of the probe-target complex. Here ferrocene-labeled reporter strands signal the presence of the target DNA hybridization to thiolated probe sequence immobilized on

the gold electrode. A number of report found in the effort to utilize the flexibility of the high surface area nanoscale electrodes to lower the detection limit based on the electrochemical readout [29–34]. In 2008, Feng et al; reported a DNA hybridization sensor to detect sequence-specific DNA detection of the phosphinothricin acetyltransferase (PAT) gene [30]. Their sensor was able to achieve a dynamic detection range from 1 pM to 1 μM with the detection limit of 0.3 pM. In 2009, Soleymani et al. have demonstrated 10 aM detection limit (using electrochemical transduction) for the first time for a label- and polymerase chain reaction-free sensor [35]. The aM sensitivity was achieved by using highly branched electrodes with fine nanostructuring. They hypothesize that this enhanced sensitivity achievable with finely nano-structure devices, the surface textures of the nanostructured electrodes enhances the accessibility during the hybridization leading to faster and more efficient binding of the analyte. Most recently (2017) a limit of detection of 67 aM was reported for nucleic acid detection by Zhang et al. using electrochemical readout [36]. In their method, in the presence of target RNA, DNA walkers are activated to walk continuously along DNA tracks, resulting in conformational changes as well as considerable increases of the signal produced by target-response and target-independent reporters. Their sensor was regenerative and stable for at least 5 cycles without the reduction in sensitivity. This is the most recent report that demonstrated aM level detection limit for nucleic acid sensing with the similar toehold-mediated strand displacement reaction employed in our thesis.

Figure 1.4 shows a schematic of a planar gold electrode (left) and nanomaterial-based electrode (right) with the high surface area that allows immobilizing more capture DNA probe to enhance the sensitivity of a target-specific hybridization sensor compare to the conventional planar electrodes. Figure 1.5 demonstrates a structure of a DNA duplex and DNA hybridization principle, showing that DNA hybridization happens by the binding

of A-T (Adenine-Thiamine) and G-C (Guanyin- Cytosine).

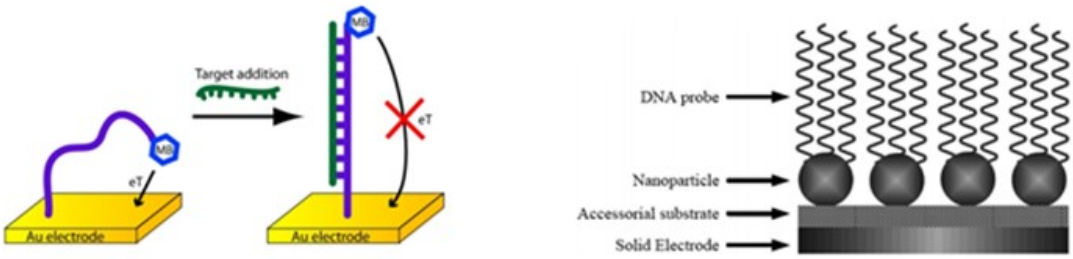

Figure 1.4: Schematic showing a dna hybridization sensor on the planar gold electrode (left) and using nanoscale high surface area electrode (right). Adapted from reference [37] with the permission from the Journal of Visualised Experiments

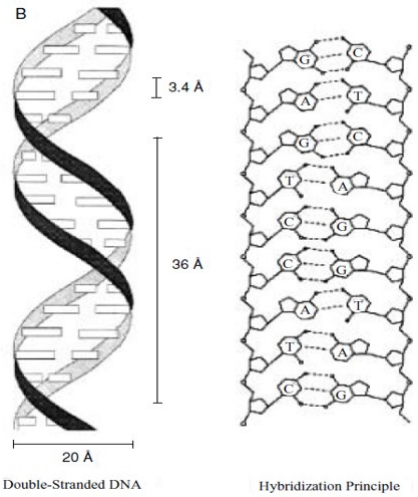

Figure 1.5: DNA structure and Hybridization principle. Adapted from reference [38] with the permission from the Springer publication.

1.3 Literature Review of Protein Sensor

Depending on the type of Bioreceptors, protein biosensors can be characterized into following five categories [38];1) Antibody/Antigen, 2) Enzymes, 3) Nucleic Acids (DNA/RNA/PNA), 4) Cellular structures/cells (i.e. microorganisms, proteins), and 5) Biomimetic (A receptor that is fabricated and designed to mimic a bioreceptor. i.e., synthetic bioreceptors). For this thesis, I have chosen to discuss on the major two receptors that widely used for protein detection (Antibody/Antigen and Nucleic Acids receptors).

1.3.1 Antibody Bioreceptor

An antibody is a complex biomolecule that consists of hundreds of individual amino acids arranged in a highly ordered sequence. These biomolecules have a very specific binding capability for specific structures. ELISA (enzyme-linked immunosorbent assay) is the widely used immunoassay to detect protein with Antibody/Antigen bioreceptor, where a target-specific antibody/antigen is immobilized on a solid surface that is linked an enzyme and detection is accomplished by assessing the conjugated enzyme activity via incubation with a substrate to produce a measurable product [39]. Though a majority of commercial ELISA kits claims the detection limits in the sub-nM range, in the literature there are a significant number of ELISA products that claim detection limits in the low pM range that employs readout strategy like Electrochemical, colorimetric, chemiluminescence [40]. Figure 1.6 demonstrates typical immunosensor formats that use antigen bioreceptor and Figure 1.7 shows label-free immunosensor formats that utilize electrochemical readout. Kerman et al. achieved up to 20 pM detection limit of the label-free electrochemical immunosensor by analyzing Square Wave Voltammetry (SWV) [41].

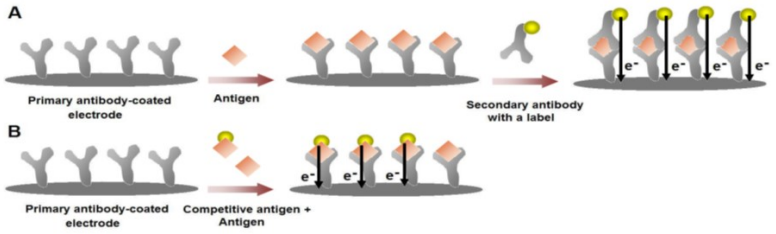

Figure 1.6: Schematic illustration for the general immunosensor formats. (A) Sandwich-type immunoassay with a labeled-secondary antibody. After the binding of the target antigen to the primary antibody-modified surface, the secondary antibody with a label is introduced to the form the sandwich-type complex. Various molecules such an enzyme or a nanoparticle can act as the source of electrochemical responses. (B) In a competitive-type immunosensor, the target molecule competes with its labeled form to attach on the primary antibodies on the surface. The electrochemical responses obtained from the labeled antigens are inversely proportional to the concentration of the target antigen. High sensitivity levels can be reached using competitive immunosensing strategies. Adapted from reference [41] with the permission from the Molecular Diversity Preservation International.

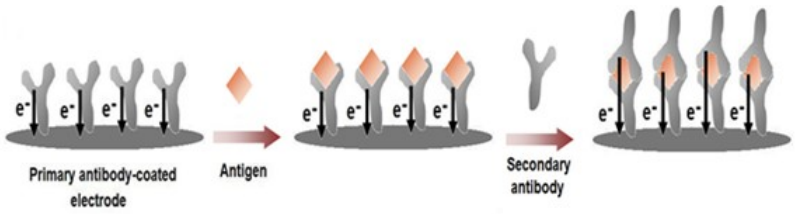

Figure 1.7: Schematic illustration for the label-free voltammetric immunosensors. The primary antibody is coated on the electrode surface, and the electro-active residues in the antibody structure give a specific current response. Upon the binding of the target antigen with the antibody, the specific current response of the antibody layer changes. This change can either be an increase or a decrease depending on the structure of the antigen and the conformational changes that would occur upon the formation of the antigen-antibody complex. Then, the current responses would be further altered with the binding of the secondary antibody, which would also contribute to the current response with its intrinsic electro-activity.Adapted from reference [41] with the permission from the Molecular Diversity Preservation International.

1.3.2 Nucleic Acid Bioreceptor for protein detection

As a bioreceptor, Nucleic acid attracted most interest in the scientific community to develop biosensors. DNA biosensors often referred as a genosensors, are developed based on the complementary of adenine : thymine (A : T) and cytosine : guanosine (C : G) pairing in DNA (Figure 1.5) defining the basis of the specificity of the biorecognition in DNA biosensors. Along with hybridization sensors, DNA-ligand interaction was also studied by different types of transduction techniques [42]. There are different types of protein detection strategies reported in the literature. Figure 1.8 shows an example where a methylene blue (MB) redox tagged thiolated DNA was immobilized and hybridized with a target specific antigen tagged complementary DNA. After the hybridization, the electrochemical signal decreases because the redox tag is now away from the electrode surface. After the target protein binding to the sensor, a signal decrement up to 80 % was achieved showing detection limit of 200 nM with this sensor. Figure 1.9 shows a schematic of protein detection strategy uses DNA as a sensor by shaded et al. Where they were able to achieve 1 nM detection limit on detecting protein. In this report, they have used steric hindrance effect as the strategy of the signal amplification. The main advantage of this novel signaling mechanism is that it remains selective enough to be employed directly in complex samples such as whole blood and remain insensitive to nonspecific adsorption of proteins on the sensor surface.

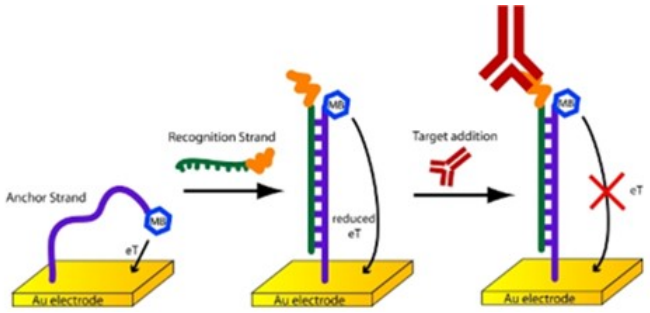

FIGURE 1.8: Schemetics of Detection principle for protein detection with electrochemical Transduction. Adapted from reference [37] with the permission from the Journal of Visualised Experiments.

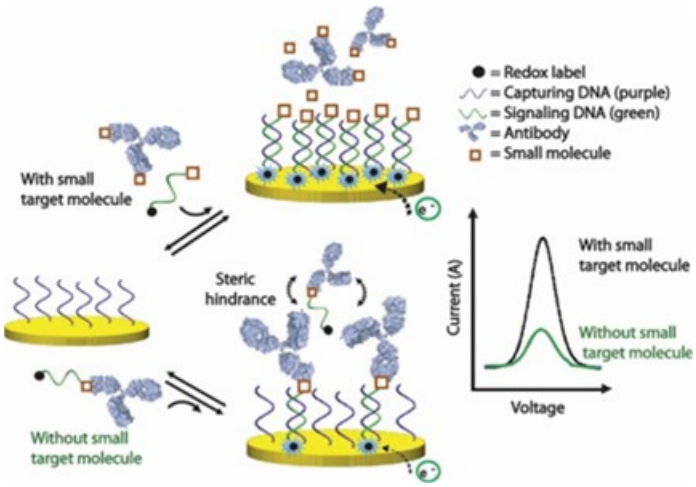

FIGURE 1.9: Schematic representation of CSA, a competitive electrochemical steric hindrance hybridization immunoassay to detect small molecules. The proposed sensor is composed of densely packed electrode-bound "capturing" DNA strands (purple), free complementary signaling DNA strands (green) dual-labeled with the target small analyte (red squire box) and a signaling redox label (black circle: methylene blue), and an antibody specific for the target molecule. In the absence of a specific analyte in the sample (bottom), the signaling strands remain bound to the antibody, which significantly reduces the ability of this large DNA complex to hybridize on the electrode surface due to steric hindrance. This ultimately generates a low electrochemical signal (blue curve). In the presence of target analytes, this later bind to the antibody and the small signaling DNA can reach the electrode surface and hybridize efficiently to most complementary capturing strands, thus generating a large electrochemical current (black curve) by bringing redox labels near the electrode's surface: Adapted from reference [43] with the permission from the ACS Publications.

1.4 Proposed Model: Protein Responsive Programmable dynamic DNA Assembly (PRPDA)

Li at al. proposed a programmable dynamic DNA assembly as tools of protein detection by employing strand displacement strategy [1]. In their work, they successfully were able to convert protein bindings to the release of a pre-designed output DNA molecules utilizing their proposed binding-induced DNA strand displacement assay using fluorescent transduction technique [1]. Figure 1.10 demonstrates dynamic assembly of DNA that programmed through a cascade of strand-displacement reaction which subsequently able to amplify the detection signal for the target molecules (Protein in this case) by releasing an intermediate fluorescent tagged DNA sequence. They hypothesized that the fluorescence signal is proportional to the target protein. PRPDA shares three main attractive features; 1) Detection of proteins can be accomplished by the detection of amplifiable DNA to improve the sensitivity dramatically, 2) Assembly of DNA is triggered by affinity binding of two or more probes to a single target molecule which increases the specificity; and 3) The assay is conducted in solution with no need for separation which has the potential for point-of-care application [1].

In this thesis, the proposed model is designed based on the concept developed by Dr. Li [1] that utilized fluorescent based transduction (illustrated in the previous Figure 1.10) to the protein detection. The significant difference is that instead of fluorescence readout we employed electrochemical readout in our model. The design illustrated in Figure 1.11 below. The binding-induced three-way junction (TWJ) strand displacement is designed to have a target recognition and signal output elements. Target recognition is achieved by two specific affinity ligands binding to the same target molecule. Two DNA motifs, TB and B*C, are each conjugated with an affinity ligand. Motif TB is designed to have a toehold domain T and a binding domain B, separated by a flexible linker of

two thymidine bases. Motif B*C has a binding domain B* and a competing domain C. TB and B*C are designed to have only 6 complementary bases (domain B and B*, green color in Figure 1.11) so that they cannot form a stable duplex at room temperature. However, in the presence of the target molecule, the binding of two affinity ligands to the same target molecule brings TB and B*C to close proximity, greatly increase their local effective concentrations [1]. Consequently, TB and B*C hybridize to each other to form a stable TB:BC* duplex. Once TB:BC* forms, it triggers a subsequent toehold-mediated strand displacement reaction with T*C*:C-MB, forming a binding-induced TWJ (TB:B*C:T*C*) and releasing the motif C-MB, which is the reporter probe (RP) modified by Methylene Blue (MB) redox agent. Hybridization of free C-MB detected on the sensor prepared by modifying a gold electrode with prehybridized complementary DNA sequence (complementary to the C-MB) carrying a toehold (capture probe, CP) using toehold-mediated strand displacement. Upon hybridization of C-MB, MB reduced near the gold surface to generate an electrochemical signal. The generated electrochemical signal is then recorded to analyze. Structure of MB and the reduction reaction shown in Figure 1.11(B) [44].

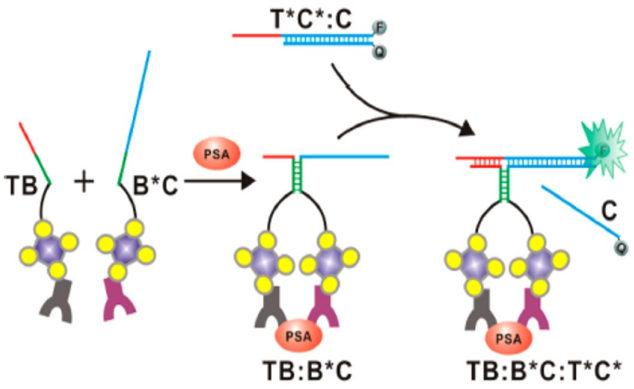

Figure 1.10: Schematic showing the design of PSA-responsive TWJ. Adapted from reference [1] with the permission from the ACS Publications.

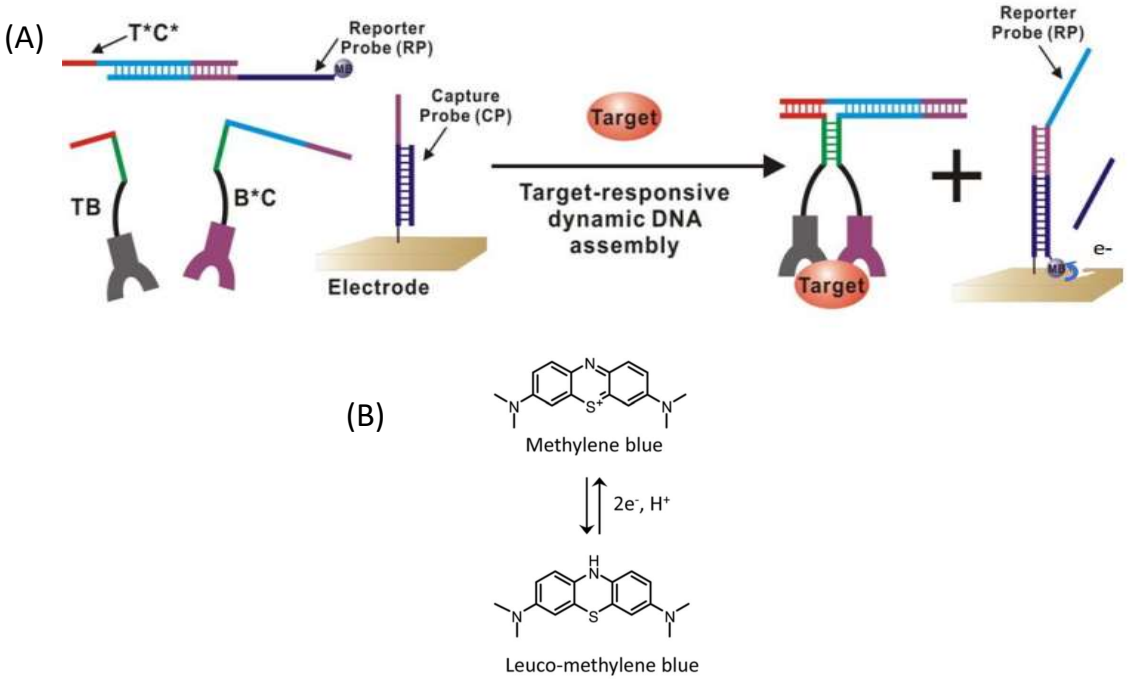

FIGURE 1.11: (A) Schematic of the proposed model, showing the principle of the binding-induced formation of DNA Three-Way Junction. Binding of the target molecule (Protein) to the two specific affinity ligands brings two DNA motifs, TB and B*C, to close proximity, forming the TB: B*C duplex. The formation of TB: B*C triggers a subsequent strand displacement between TB:B*C and C-RP-MB, resulting in a stable binding-induced TWJ (TB:B*C:T*C*) and the release of C-RP-MB. This redox strand will then be captured by the capture probe (CP) immobilized in the electrode by means of DNA strand displacement assay. An electrochemical readout technique will be employed to detect the reporter probe, RP.(B) Shows the Mathelene Blue reduction reaction.

1.5 Research Objective

The primary objective of this thesis is to achieve a lower limit of detection (LOD) using PRPDA assay with electrochemical readout compare to the LOD reported (2.8 nM) by Li. et al.[1] using fluorescent transduction technique that uses similar PRPDA strategy to detect protein. To meet the primary objective in the end, the following more specific goal was pursued:

- To determine a voltammetry technique that can provide the highest signal to noise ratio.
- To determine the scanning solution that can provide the highest signal to noise ratio in the electrochemical measurement.
- To lower the limit of detection (LOD) of MB labeled DNA with strand displacement assay, which is an essential intermediate step in detecting protein via PRDS assay.
- To minimize the background signal that occurs due to nonspecific adsorption of redox marker to the gold electrode surface due to non-affinity binding.
- To minimize the background signal caused by the unwanted formation of three-way-junction (TWJ).

1.6 Thesis Overview

The remainder of the thesis is organized as follows.

Chapter 2. provides a brief background on electrochemical setup and instrumentation with the theoretical background on the electrochemical techniques used in this thesis. This chapter also illustrates the experimental protocol used in this experiment to develop the hybridization sensor prepared on gold electrode surface that is essentially the final step of the PRPDA protein detection scheme.

Chapter 3. elaborates the major findings towards the development of the PRPDA protein detection scheme to lower the limit of detection utilizing electrochemical read-out. The experiments presented includes characterization of the hybridization sensor developed in the gold electrode surface, determination of the scanning solution that has potential to provide a large signal to noise ratio, development of the strand displacement assay, minimization of nonspecific adsorption and unwanted hybridization. Finally demonstrates that by utilizing the high surface are a wrinkled electrode, LOD can be pushed further compare to planar for the PRPDA protein detection assay.

Chapter 4 illustrates major contribution to the field by discussing the new findings and the impact of this work in the broader view. This chapter concludes by summarizing the major findings of the thesis by providing insight of the gaps and shortcoming of this work to point the scope of the future work to be done to improve the LOD utilizing PRPDA protein detection scheme.

Chapter 2

Experimental Apparatus and Procedures

2.1 Instrumentations

This section discusses the major apparatus and the electrochemical methods used to perform electrochemical bio-sensing experiments. The electrochemical techniques used in our experiments are Cyclic Voltammetry (CV), Differential Pulse Voltammetry (DPV), Square Wave Voltammetry (SWV).

2.1.1 Electrochemical Setup

Three-electrode based electrochemical potential setup consists of a Reference Electrode (RE), Working Electrode (Working Electrode (WE)) and a Counter Electrode. A potential is applied between the RE and the WE and the resultant current is measured between the WE and the Counter Electrode (CE). Figure 2.1 shows the schematic of a typical three-electrode system.

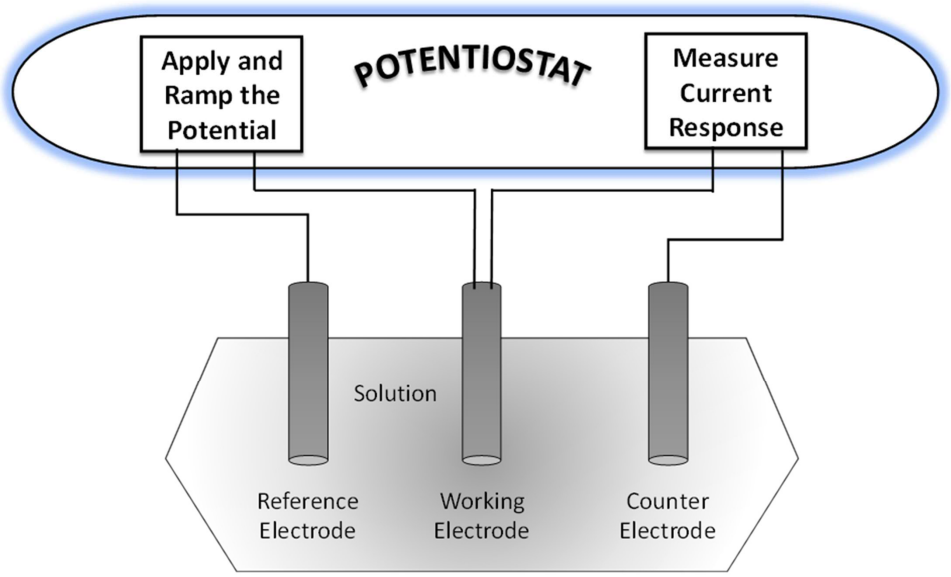

Figure 2.1: Potentiostat with the three-electrode configuration for performing electrochemical measurements.

2.1.1.1 Reference Electrode (RE)

The reference electrode (Reference Electrode (RE))is an electrode that has a well-known and stable electrode potential. A standard Ag/AgCl with a potential of 0.230 V vs. standard hydrogen electrode (SHE) [45] was used as reference electrode. Due to a high impedance between the working electrode and the reference electrode, a negligible current is possessed to avoid a drop in the potential. Figure 2.2 shows a Ag/AgCl reference electrode.

FIGURE 2.2: photo of an Ag/AgCl reference electrode.

2.1.1.2 Counter Electrode (CE)

Platinum (Pt) electrode was used as a counter (or auxiliary) electrode. To allow the reference electrode to keep its high impedance condition, the resultant current produced due to the redox reaction passes across the working electrode and the counter electrode. The size of counter electrodes is usually larger compare to the WE's. Figure 2.3: Photo of a Pt counter electrode used in this experiment.

FIGURE 2.3: Photo of Platinum reference electrode.

2.1.1.3 Working Electrode(WE)

The working electrode is which modified to prepare the sensor. Sensor performance was analyzed between the planar gold electrodes and the wrinkled gold electrodes. Planar gold electrodes were purchased form CHI. Wrinkled electrodes were prepared electroless prepared by the protocol developed in our lab. Figure 2.4 shows a photo of planar gold macro electrode (A), (B) Photo of wrinkled micro electrode prepared via electroless god deposition and (C) Scanning Electron Microscopy images of the working surface employed to develop the electrochemical DNA hybridization senso,

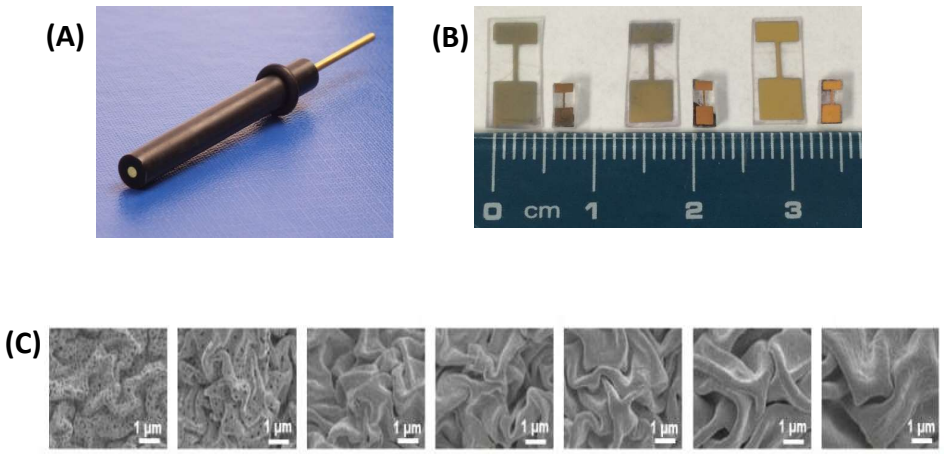

Figure 2.4: (A) Photo of planar gold macro electrode. (B) Photo of wrinkled micro electrode prepared via electroless god deposition and (C) Scanning Electron Microscopy images of the working surface employed to develop the electrochemical DNA hybridization sensor

2.2 Procedures and protocols

2.2.1 Materials and reagents

The following reagents were purchased from Sigma-Aldrich (St. Louis, Missouri); Potassium Chloride (KCl, $\geq$ 99.0%), Phosphate Buffered Solution (PB solution, 1.0 M, 7.4 pH), 6-mercapto-1-hexanol (MCH, $\geq$ 99.0%), hexaaammineruthenium (III) chloride (RuHex, 98%), potassium hexacyanoferrate (II) trihydrate (FoCN, 98.5%). Potassium ferricyanide (FiCN, 99.0%) was purchased from Anachemia (Rouses Point, NY). Sulfuric Acid (H_2SO_4, 98%), 2-propanol (99.5%), sodium chloride (NaCl, $\geq$ 99.0%), methanol ($\geq$ 99.8%) were purchased from Caledon Laboratories (Georgetown, Ontario). Ethanol was purchased from Commercial Alcohols (Brampton, ON). Sodium Hydroxide was purchased from LabChem Inc. (Zelienople, PA). Tris-EDTA (TE Buffer, pH = 8.0) and Tris-(2-Carboxyethyl)phosphine, hydrochloride (TCEP) were purchased from Thermo Scientific (Rockford, Illinois). Tris(hydroxymethyl)aminomethane (tris, $\geq$ 99.9%) was purchased from BioShop Canada (Burlington, ON). All other reagents were of analytical grade and were used without further purification. Milli-Q grade ultrapure water (18.2 MΩcm) was used to prepare all solutions and for all washing steps.

2.2.2 DNA sequences

The oligonucleotide sequences listed below were synthesized from the Biosearch technologist.

P1 (t-RP-SH): **5'-TAC ACG CTT GAG AGA CTG ATT GGA AGA SH -3'**

D1 (P*): **5'-TCT TCC AAT CAG TCT CTC AA -3'**

U3: **5'-TTT TTT TTT TTT TTT TTT TTT TTT TTT TTT TTT TTT TTT TT–3'**

L2 (CR*-MB): **5'-MB TCT TCC AAT CAG TCT CTC AAG CGT GTA TCC CAT GTG TC - 3'**

T*C*:5'-CTA GAG CAT CAC ACG GAC ACA TGG GA-3'

TB: 5'-BiotinTEG/ TTT TTT TTT TTT TTT TGT GAG-3'

B*C: 5'-BiotinTEG/AAG CGT GTA TCC CAT GTG TCC CTC ACT-3

L3: **5'–MB TTT TTT TTT TTT TTT TTT TTT TTT TTT TTT TTT TTT TT – 3'**

2.3 Electrode Preparation

2.3.1 Planar Electrode Preparation

Planar gold disk macroelectrodes were prepared for the sensor modification. Macroelectrodes were polished with CarbiMet to remove any large scratch present on the electrode surface, followed by cleaning in the flow of DI water. Next, electrodes were polished with 0.3 um alumina beads on a polishing cloth damp with DI water, sonicating for 5 minutes each in ethanol and then DI water, and repeating polishing and sonicating with 0.05 um alumina beads, followed by sonicating using the same condition. A picture of a sonication station shows in the picture in the Figure 2.5 below.

Figure 2.5: Picture of the sonication station.

A CV scan in 0.05 M H2SO4 was performed to electrochemically polish the surface.

An applied potential of 0V to +1.5 V was employed with a scan rate of 0.1 V/s for 80 cycle electrochemical polishing. Afterwards, bare scans were taken as a baseline measurement a bare gold surface modification. A picture of electrochemical station during CV scan is shown in Figure 2.6.

This technique is due to the oxidation and reduction of an adsorbed layer of gold oxide at the surface of the gold. A representative cyclic voltammogram of a sulfuric acid scan of a planar gold surface is shown in Figure 2.7 below. Between +1.0 V and +1.5 V, the oxidation of gold occurs. Upon a reversal in scan polarity, a reduction reaction occurs indicated by a characteristic peak at approximately +0.83 V. The electro-active surface area may be determined from the charge associated with the reduction current by integrating the peak area, and dividing this value by the surface charge density of gold (386 μC/cm2).

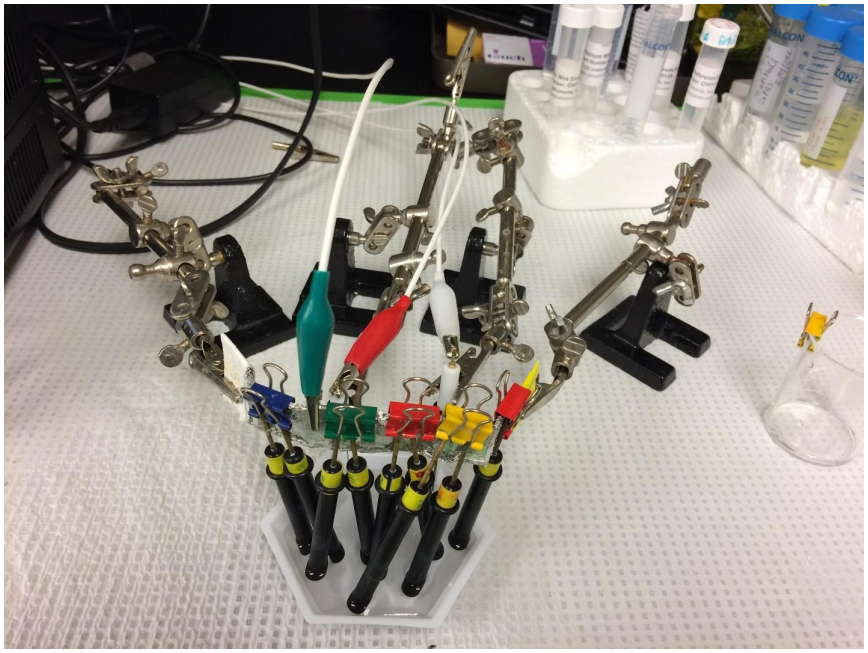

FIGURE 2.6: Multiple electrodes can be electrochemically cleaned together. This should be followed by performing H_2S0_4 scans per individual electrode. The electrode holder seen above is created with aluminum foil, clips and tape, held by two helping hands.

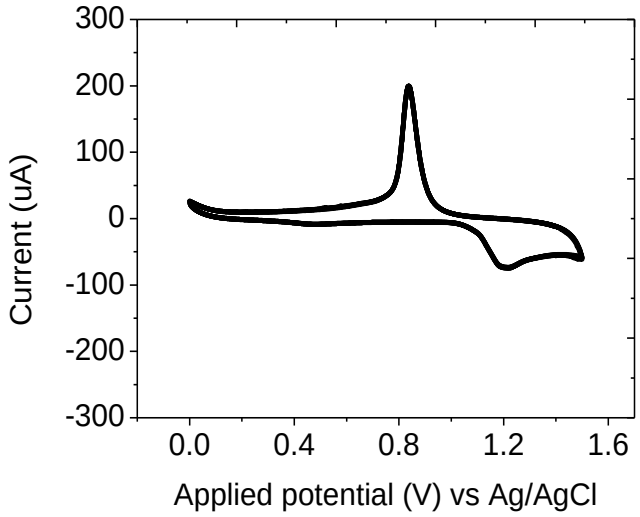

Figure 2.7: Voltammogram of Sulfuric Acid CV scan for electrochemical polishing.

2.4 Surface Modification protocol

2.4.1 Thiol Reduction

Probe DNA Received in lyophilized form, which was resuspended with 1 X TE buffer to 1 mM concentration and 25 μL aliquots were created and stored at -80 °C for long term use. Next, disulfide bond of the 5' modifier on the probe DNA, P1, was cleaved to reveal the thiol to immobilize the probe DNA on the Au surface by means of thiol-on-gold self-assembled monolayer. Following series of steps were performed to cleave the dithiol: 50 μL of a 10 mM TCEP solution (Stock solution was prepared from TCEP powder) was added to 25 μL of unreduced probe DNA. The mixture was left at the room temperature for the reduction reaction to complete for 1 hour followed by vortex briefly. The thiol reduced solution then transferred to a 3 kDa Nanosep spin column with 150 μL of a 100 mM NaCl and 10 mM PB solution (100/10) for filtering the unwanted residues. Filtration was performed for 15 minutes at 8.6 kRPM and repeated the step 3 times to get better filtration. After the spinning, 75 μL of 1000/10 was added to the retentate and spun at the same conditions for 15 minutes. The retentate was collected in a small tube with 75 μL of 1000/10 solution and stored in 4 °C. This solution was diluted with 25 mM NaCl, 25 mM PB solution and 100 mM Mg_2Cl_2 to a concentration of 1 μM to create the probe deposition solution.

2.4.2 Probe Quantification

Quantification of the reduced probe DNA concentration was performed in a UV-vis instrument. 15 μL of reduced probe DNA was added to 185 μL of a solution containing 100 μM 5,5-dithio-bis-(2-nitrobenzoic acid / Ellman's Reagent (DTNB), 0.1 M PB solution, and 1 mM EDTA to a UV-transparent 96-well plate. A blank was created by adding

15 μL of 1000/10 to 185 μL of the same solution. Reduction efficiency was then determined by comparing DNA concentrations from 260 nm (Native DNA absorbance) and 410 nm (thiol-DTNB absorbance) absorbance reading. 70 to 95 % reductuion efficiency was found with this protocol.

2.4.3 Probe Deposition

The electrodes were washed in flow of DI water and placed in to individual 50 mL falcon tubes, such that electrode surface was facing upwards on Styrofoam in the bottom. To limit the evaporation, a humidity chamber was created by placing sufficient water into the tubes. Previously prepared thiolated probe was diluted to 1 μM, and 5 μL of probe deposition solution was placed onto each electrode, tube was capped to seal and protect the internal environment. Probe deposited electrodes were then placed into 4 °C overnight to form thiol on gold surface assembled monolayer. Next morning, electrodes were removed from the chambers and washed with 25/25 (25 mM NaCl and 25 Phosphate Buffer (PB) solution) and DI water respectively. Then, Electrodes were put back into the falcon tubes (humidity chamber). 5 μL of 1 mM MCH solution was then placed onto the electrode surface for the backfill step for 4 hours at room temperature. Electrodes were then washed with 25/25 followed by rinsing in DI water.

2.4.4 Hybridization

Electrodes were returned to humidity chamber created falcon tubes, and 5 μL of desired hybridization (target) solution was placed onto the electrode surface. Which were then incubated at 37 °C. for desired hybridization period depending on the experiment performed. Electrodes were washed with 25/25 and flow of DI water before taking the target electrochemical scans.

2.4.4.1 Duplex preparation

Duplex (T*C* : RP-MB and P1 : D1 = CP) was prepared by following protocol using thermal cycler. In a tube 12.5 μL of T*C* / P1 and 12.5 μL of RP-MB / D1 were mixed in 1:2 (MB-RP : T*C* / P1 : D1) ratio. 25 μL of the mixed solution then put on the thermal cycler chamber followed by slightly vortex the mixture. Thermal cycler was pre-programmed such a way that it heats the sample to 95 °C then increase the temperature difference to 5 °C with a time interval of 2 min till reach the sample to room temperature (25 °C).

2.4.4.2 Three way junction (TWJ) preparation

Dithiol of the P1:D1 duplex was reduced by following the protocol explained in the section 2.2.1. Thiolated P1:D1 duplex then diluted to 1 uM with the probe deposition buffer (25/25/100). 5 μL of 1 μM thiolated duplex probe was deposited on planar disk gold electrodes and 3 μL was deposited on wrinkled gold electrodes overnight to form thiol on gold self-assembled monolayer capture probe (CP). Probe scans were taken following the protocol stated in the section 2.2.1.

To prepare the blank solution, biotin modified intermediate strands, TB and BC, protected toehold reporter probe, T*C*: RP-MB were diluted to desired concentration with 25/25/100. In a different tube, target solution was prepared by adding target streptavidin protein to the blank solution. A set of 3 electrodes were used for both planar and wrinkled electrodes.

Respective experimental protocol is discussed in the individual experiment.

2.5 Readout Techniques

2.5.1 Cyclic Voltammetry

Cyclic Voltammetry (CV) is a potential sweep technique which can be employed to study electron transfer kinetics and transport properties of electro-catalysis reaction on the electrodes surface. In a three-electrode system, a linearly increasing potential with time (scan rate (V/s)) applied between the reference electrode and working electrode (Figure 2.8, top). Concomitantly, the resultant current is measured between the working and counter electrode. The resulting data then plotted as current (i) vs potential (E) (Figure 2.8, bottom). Observed reduction and oxidation events are shown in the resulting plots. Reduction events occur at analyte specific potential voltages where the reaction $A + e^- \rightarrow A^-$ (A = Analyte) is energetically favored (known as reduction potential) and measured by increasing current values. Current increases till the applied potential reaches the reduction potential of the analyte, but then falls off as the maximum rate of mass transfer has been reached. The current decreases till the reaction reaches to a equilibrium at some steady value. Oxidation reaction ($A^- - e^- \rightarrow A$)) is also observed as decrease in current values at the potentials that energetically favor the loss of electrons.

The resulting voltammograms are analyzed and the potential (Reduction potential, E_{pc} and Oxidation potential, E_{pc}) and current (Reduction current, I_{pc} and Oxidation current, I_{pa}) data for both reduction and oxidation events based on the surface modification. These are the fundamental parameters used to characterize a redox event. The oxidized and reduced forms of a compound are in equilibrium at the electrode surface. The relationship between potential and the equilibrium ($\frac{[R]}{[O]}_{x=0}$) can describes by the

Nernst equation.

$$E = E^0 - \frac{RT}{nF} ln \frac{R}{O}_{x=0} \tag{2.1}$$

Where, $E^0 = \frac{E_{pa}+E_{pc}}{2}$ is called the formal potential of the reaction and considers the activity coefficients and other experimental factor.

Specifically, the peak current of a reversible reaction is given by:

$$i_p = (2.69 \times 10^5) n^{3/2} A D_0^{1/2} v^{1/2} C_0^* \tag{2.2}$$

Where, i_p is peak current in amperes, n is the number of electrons involved, A is the area of electrodes in cm^2, D_0 is the diffusion constant (cm^2/s), v is the scan rate (V/s) and C_0^* is the bulk concentration ($moles/cm^3$). In this thesis $FiCN_4$ was used as an Electrolyte solution.

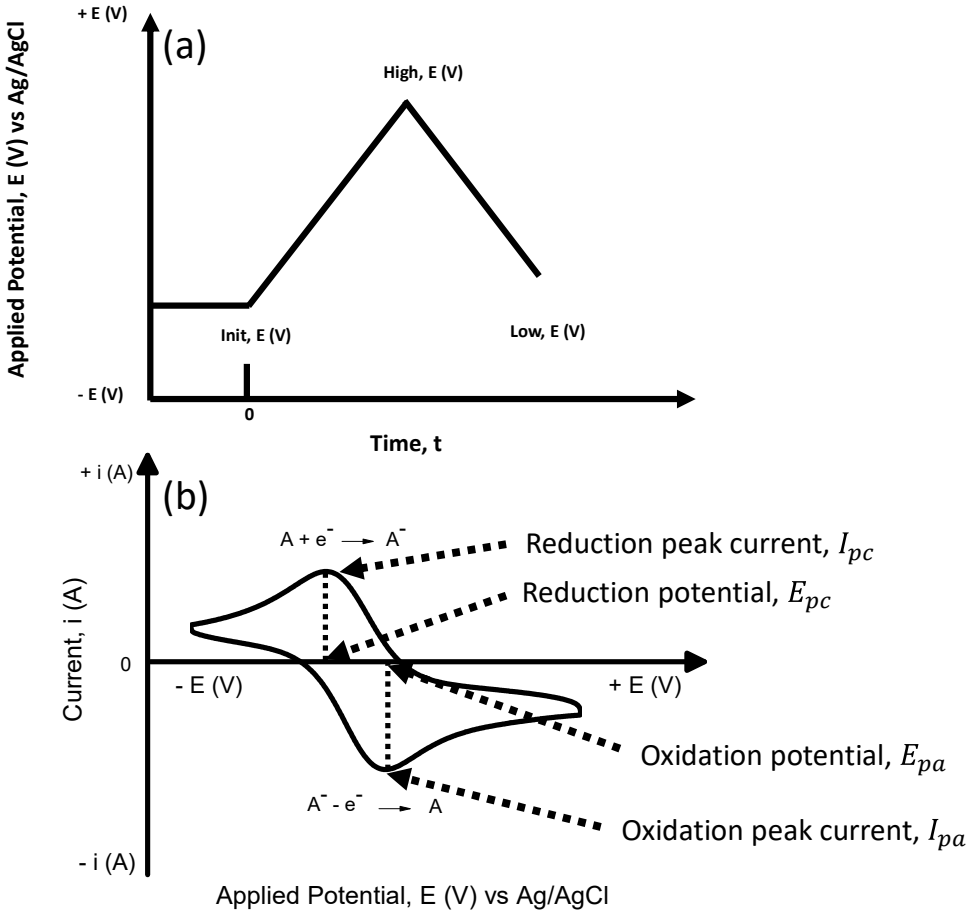

FIGURE 2.8: Schemetic of applied potential (a) and a sample i-v curve (b) of a Cyclic Voltammetry

2.5.2 Differential Pulse Voltammetry

Differential pulse voltammetry (DPV) is a voltammetric technique, where a series of pulses applies in the working electrode such that the base potential is incremented between pulses and the increments are equal. Difference between the current just before the application of the pulse and at the end of the pulse is recorded. Resulting current vs. applied potential are then plotted for the analysis. Farley long waiting period before the new pulse applied, allows to discharge the capacitive current occurs between electrode and electrolyte interface. Current magnitude and potential of the redox peaks are the two-important information can be observed from a DPV signal. The height of the current peak, I_{pc} is directly proportional to the concentration of corresponding analyte, C. Which can be expressed as, $I_{pc} \propto$C. It has been demonstrated that Square Wave Voltammetry (SWV) could be four times more sensitive than DPV [46]. Rapid scanning capability and the reversal nature of SWV is also beneficial for the kinetics study. Figure 2.9 shows a Schemetic of applied (left) potential and a sample DPV voltammogram (right).

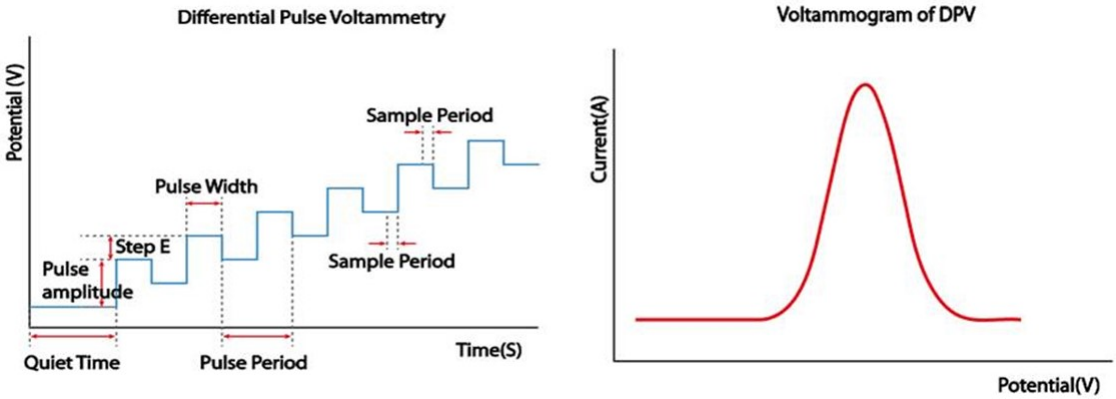

Figure 2.9: Schemetic of applied (left) potential and a sample DPV voltammogram (right).

2.5.3 Square Wave Voltammetry

Square Wave Voltammetry (Square Wave Voltammetry (SWV)) is a large-amplitude differential technique, in which a waveform composed of symmetrical square-wave, superimposed on a base staircase potential, which is applied to the working electrode (Figure 2.10, left) [47]. The current is measured twice for every square wave cycle (once at the end of the forward pulse and another at the end of the reverse pulse) and their difference is plotted against the base staircase potential. Large modulation amplitude of the square-wave allows the reverse reaction to occur of the product of the forward pulse. This is an advantage over the DPV that in DPV, it requires to wait a certain period of time to reach analyte to the close to electrode surface from the bulk. The peak current is proportional to the concentration of analyte. Oxidation and reduction current measurement in consecutive waves in a high pulse rate always provides a high net current, which makes SWV a extremely sensitive technique. Figure 2.10 shows a Schemetic of applied (left) potential and a sample SWV voltammogram (right).

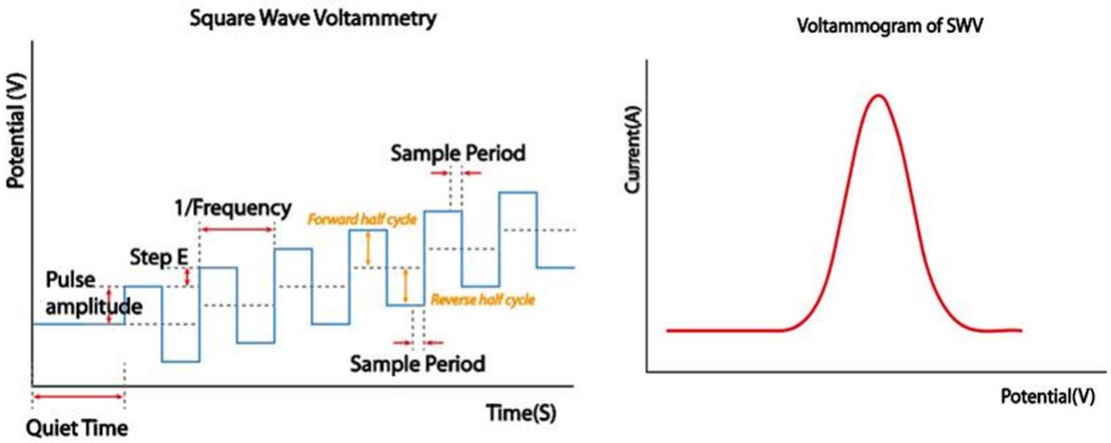

Figure 2.10: Schemetic of applied (left) potential and a sample SWV voltammogram (right).

2.5.4 Alternate Current Voltammetry

Alternate Current Voltammetry (Alternate Current Voltammetry (ACV)) consists the superimposition of small amplitude AC voltage on a linear ramp. The frequency of an AC potential is usually ranges from 50 - 100 Hz at an amplitude of 10 - 20 mV. For a reversible reaction, the height of the ACV perak is proportional to the square root of the frequency (ω):

$$i_p = \frac{n^2 F^2 A \omega^{1/2} D^{1/2} C \Delta E}{4RT} \tag{2.3}$$

The peak width is independent of the AC frequency and is 90.4 mV per electron exchange.

Figure 2.11 shows a Schemetic of applied (left) potential and a sample ACV voltammogram (right).

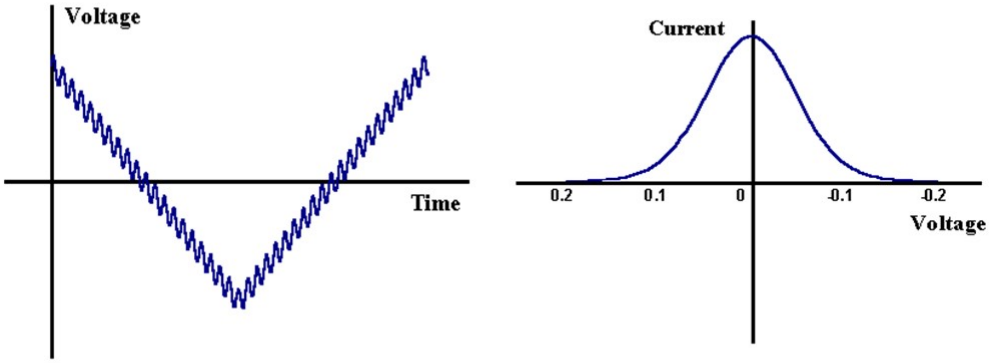

Figure 2.11: Schemetic of applied (left) potential and a sample ACV voltammogram (right).

Chapter 3

Results and Discussion

3.1 Introduction

The vision of this thesis is to develop an assay based on protein-responsive programmable dynamic DNA assembly (PRPDA). As illustrated in section 2.2, PRPDA allows detecting proteins via an intermediate process involving nucleic acids. PRPDA has previously been designed for sensitive protein analysis in fluorescent assay formats [1]. However, to further push the detection limit and to achieve assay miniaturization and multiplexing, we sought to combine PRPDA with electrochemical readout. We expect to decrease the limit-of-detection of this systems for the detection of protein biomarkers by employing high surface area wrinkled gold electrodes.

We prepared the sensor by modifying a planar gold electrode with thiolated DNA by means of thiol-on-gold self-assembled-monolayer. A cyclic voltammogram was analyzed to characterize the surface modification. A hybridization experiment was performed with and without redox modified complementary target. Next, a toehold-mediated strand displacement hybridization assay was studied by modifying the planar gold electrode.

We demonstrated protein detection using PRPDA assay for 2 μM protein (Streptavidin) target with electrochemical readout. We choose intermediate sequence TB=BC=500 nM, T*C* : CR*-MB = 500 nM (Section 1.4, Figure 1.11-A) proposed by Li et al. that optimized for the similar PRPDA assay developed for the protein (PSA) detection using fluorescence readout [1].

Square Wave Voltammogram was performed in the presence (Target) and absence (Blank) of the protein target in the buffer solution (25 mM NaCl and 25 mM PB solution). Figure 3.1 shows the results of this experiments showing similar peak current for both target and blank with a peak shift (The peak shift could arise due to the slight variation of pH in the buffer solution.). According to the proposed model demonstrated in section 1.4, SWV current observed in the absence of the protein target should not be present since the toehold-mediated strand displacement reaction is not initiated to release CR*-MB reporter probe. Hence, no redox peak should be seen. We hypothesize the peak observed here for Blank is due to the following reasons- 1) The intermediate sequence concentration was high enough to thermodynamically initiate the toehold-mediated strand displacement reaction to release the reporter probe. 2) Reaction time for PRPDS assay is long enough to initiate the strand displacement of the reporter probe. 3) MB redox reporter could be nonspecifically bound to the freely accessible gold surface. To reduce the false positive signal, we addressed these hypotheses by optimizing the intermediate sequence TB=BC, probe sequence T*C*: CR*-MB, the reaction time to release the reporter probe from the PRPDS system, and introduced poly-A in the target solution.

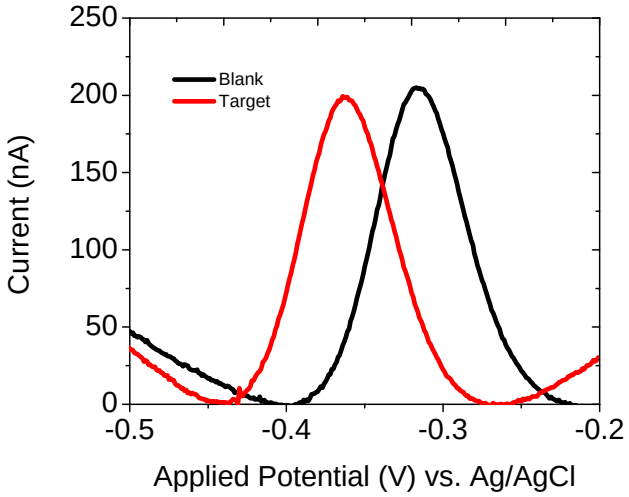

FIGURE 3.1: PRPDA assay for 1 uM protein target on the planar gold electrode with 500 nM TB=BC, T*C*: CR*-MB and 1 uM capture probe. Results show no peak current change for the target compares to the Blank.

3.2 Sensor Characterization

The goal of this experiment is to characterize the electrode surface modification with the capture probe (CP in the proposed model, Figure 1.11-A), which is essentially the sensor for the PRPDA protein detection system. Using hybridization experiment, this was demonstrated for both label-free and labeled target.

3.2.1 Label-free DNA Hybridization

Schematic in Figure 3.2 demonstrates the hybridization experiment steps for the label-free DNA target. A bare gold electrode was modified with a thiolated single-stranded DNA complementary to the target called probe. The sensor then challenged with complementary (Figure 3.2-a), and non- complementary target (Figure 3.2-b). Protocol for this experiment is described in section 2.2. Cyclic Voltammetry (CV) permits an understanding of the state of the electrode surface modification by characteristics of the redox processes at the electrode surface. Monolayer formation can be monitored via attenuation of an anionic redox agent such as Ferrocyanide, $[Fe(CN)_6]^{4-}$ [48]. Fewer faradic processes take place because of the repulsive electrostatic interactions between the anionic $[Fe(CN)_6]^{4-}$ redox reporter and the negatively charged DNA probes. The interaction is schematically illustrated in Figure 3.3.

Figure 3.4 shows the CV of the bare planar gold surface, probe-MCH monolayer modified surface, and target hybridized monolayer surface in the $[Fe(CN)_6]^{4-}$ solution. As discussed in section 2.5.1, a well-defined reduction and oxidation peaks (I_{pc} = 6.56 μA, E_{pc} = 0.175 V, I_{pa} = -7.80 μA, E_{pa} = 0.247 V) of $[Fe(CN)_6]^{4-}$ were observed with a peak-to-peak s6eparation ($Ep - p$) of 72 mV, which is the evidence of highly reversible redox reaction [49]. A sharp peak indicates that reduced/oxidized species diffuse rapidly

into or away from the solid-solution interface. After probe (P1) deposition, followed by MCH backfill, resultant CV shows a wider peak separation of 298 mV with lower reduction/oxidation peak current amplitude (reduction current, $I_{pc} = 1.64$ μA, reduction potential, E_{pc} = 0.115 V, Oxidation Current, I_{pa} = 4 μA, Oxidation potential, E_{pa} = 0.413 V). This suggests that due to repulsive electrostatic interactions between the anionic $[Fe(CN)_6]^{4-}$ redox marker and the polyanionic P1 probes (negatively charged phosphate groups of the DNA backbone) as well as DNA/MCH monolayer, which act as a physical blocking layer, fewer faradic process take place with slower reaction kinetics [48]. Upon introduction of the complementary target DNA (D1), the blocked layer exists as before, but now, because hybridization occurred, there is duplex DNA present on the surface. A more anionic phosphate backbone increases the electrostatic repulsion of $[Fe(CN)_6]^{4-}$ resulting further decrease in reduction/oxidation currents ($I_{pc} = 1.41$ μA, $Epc = 0.049$ V, $I_{pa} = 3.87$ μA, $E_{pa} = 0.489$ V) and widening peak separation (440 mV) [50]. After exposure to non-complementary target, U3 (Figure 3.4-b1), a lower peak to peak separation (177 mV) with higher reduction/oxidation peak current amplitude ($I_{pc} = 2.795$ μA, $E_{pc} = 0.134$ V , $I_{pa} = 4.63$ μA , $E_{pa} = 0.311$ V) was seen compared to corresponding probe/MCH CV results ($I_{pc} = 2.22$ μA , $E_{pc} = 0.079$ V , $I_{pa} = 4.06$ μA, $E_{pa} = 0.409$ V, $E_{p-p} = 330$ mV). Figure 3.4 (a2) and (b2) shows the peak current amplitude analysis for the 3 trials. Peak reduction/oxidation current and voltage for the label-free complementary and non-complementary target on the gold surface are summarized the table 3.1 below.

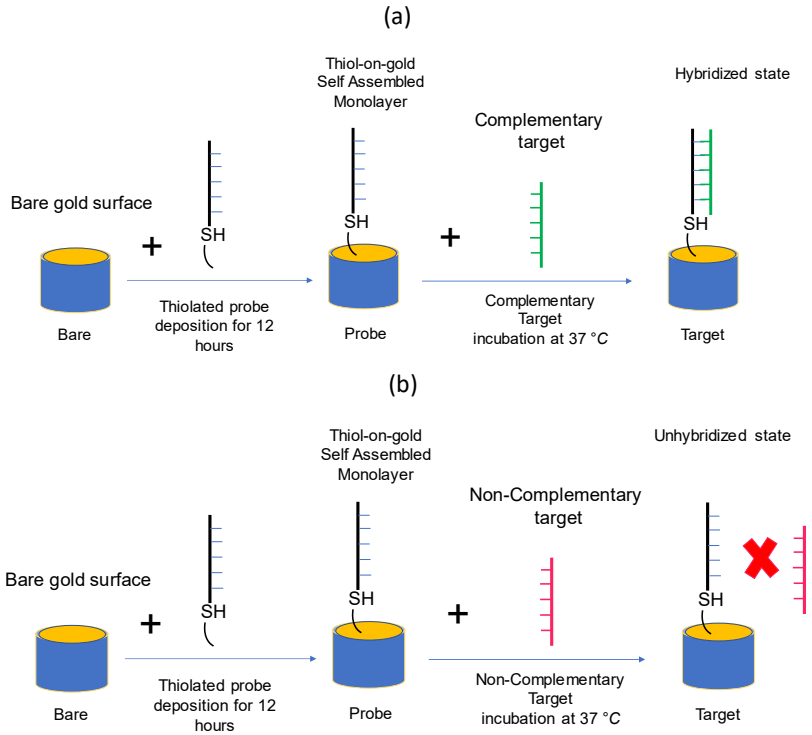

Figure 3.2: Schematic demonstrates the hybridization experiment steps for the label free DNA target. The Bare gold surface was modified with a thiolated probe using thiol-on-gold self-assembled monolayer. Hybridization state for complementary (a) and noncomplementary target (b) state was demonstrated.

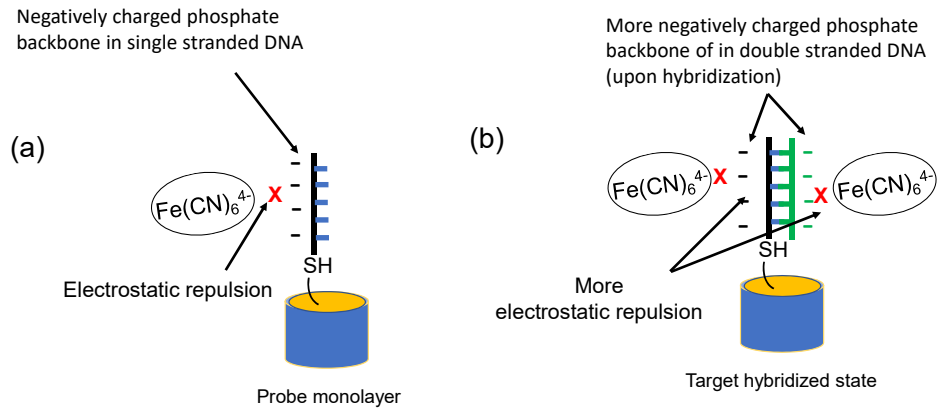

Figure 3.3: Schematic demonstrates the electrostatic repulsion between negatively DNA phosphate backbone and negetivley charged Ferrocyanide before (a) and after hybridizatoin (b).

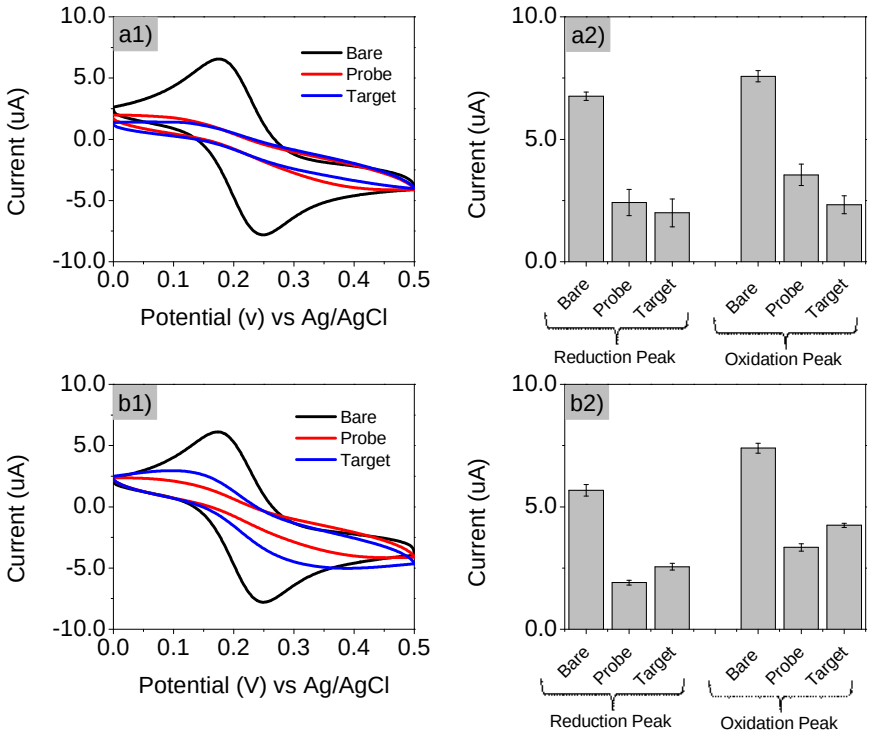

Figure 3.4: a1 and b1 are the Representative cyclic voltammogram, a2 and b2 are the oxidation and reduction peak for complementary and non-complementary targets respectively, for Bare, Probe-MCH monolayer and the Target hybridization state. Hybridization was performed with (a)1 μM complementary target, D1 and (b)1 uM noncomplementary target, U3. CV was performed in 25 mM PB solution, 25 mM NaCl and 2 mM $[Fe(CN)_6]^{4-}$ with scan setting shown in section 2.2. Error bars show a Standard error for the 3 trials.

Table 3.1: Peak reduction/oxidation current and voltage for the label-free complementary and non-complementary target modification on the sensor surface

Complementary Target	Bare	Probe	Hybridized state
Reduction Current, I_{PC}	6.56 μA	1.64 μA	1.41 μA
Oxidation Current, I_{Pa}	-7.80 μA	-4 μA	-3.87 μA
Reduction Voltage, E_{PC}	0.175 V	0.115 V	0.049 V
Oxidation Voltage, E_{Pa}	0.247 V	0.413 V	0.489 V
Peak to Peak separation, E_{p-p}	0.072 V	0.298 V	0.440 V
Non-Complementary Target	**Bare**	**Probe**	**Un-hybridized state**
Reduction Current, I_{PC}	6.56 μA	2.2 μA	2.795 μA
Oxidation Current, I_{Pa}	-7.80 μA	-4.63 μA	-4.63 μA
Reduction Voltage, E_{PC}	0.175 V	0.135 v	0.135 V
Oxidation Voltage, E_{Pa}	0.247 V	0.311 V	0.0.311 V
Peak to Peak separation, E_{p-p}	0.072 V	0.330 V	0.177 V

3.2.2 Labeled (MB) DNA Hybridization

Upon binding with a Protein target, PRPDA assay releases a Methylene Blue (MB) modified single-stranded DNA. In this section, we validated that this released MB modified DNA is complementary to the sensor sequence. Schematic in Figure 3.5 demonstrates the hybridization experiment steps for the MB labeled DNA target. A bare gold electrode was modified with a thiolated single-stranded complementary DNA to the target called probe, then a complementary (Figure 3.5-a) and non- complementary target modified with MB (Figure 3.5-b) were introduced. Surface modification protocol for this experiment is illustrated in section 2.2. Figure 3.6 shows the electrostatic repulsion between anionic $[Fe(CN)_6]^{4-}$ and anionic DNA backbone.

Investigation of CV for the Bare, Probe/MCH monolayer and MB labeled target hybridization shows (Figure 3.7) similar properties as label-free target hybridization described in the previous section. Properties including, widening of the peak to peak separation, 81 mV, 189 mV and 214 mV and decrement of the peak current amplitude for Bare, Probe and Complementary MB modified Target, L2 (Figure 3.7-a1, a2) hybridized state respectively. In this experiment both, $[Fe(CN)_6]^{4-}$ and MB (oxidized form) are present in the solution. However, since redox potential of MB (-0.3 V) does not coincide with the potential window for CV scan (0 to 0.5), MB does not participate in the redox reaction. We hypothesize that freely available oxidized MB (positively charged) could attract the anionic, $[Fe(CN)_6]^{4-}$ facilitating the increase of charge transfer rate during the redox reaction [51]. Due to the increased charged transfer rate, E_{p-p} shows less change (25 mV) in the presence of MB compare to a larger E_{p-p} of 142 mV observed (for the label-free target) when $[Fe(CN)_6]^{4-}$ present alone in the solution. This hypothesis is also support for the non-complementary target showing less E_{p-p} change in the presence MB (4 mV) compared to the large E_{p-p} change of -112 mV calculated for the label-free non-complementary target. Reduction/oxidation peak current and voltage for the MB

labeled complementary, and the non-complementary target is summarized in table 1.2.

This experiment suggests that both label-free and MB labeled complementary DNA sequence can be differentiable with the developed sensor.

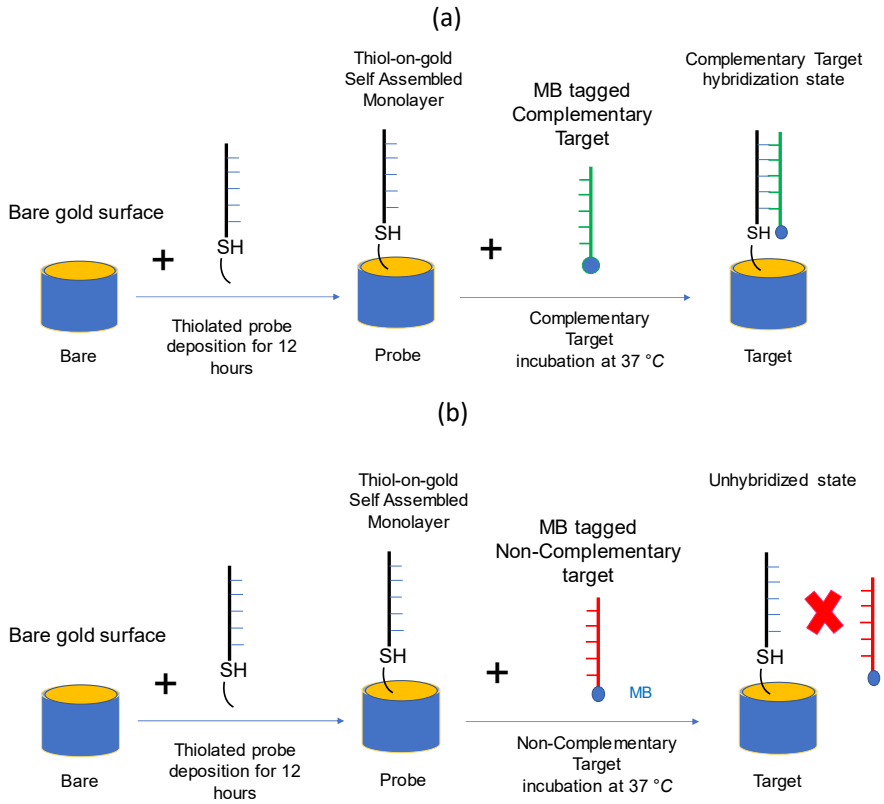

Figure 3.5: Schematic demonstrates the hybridization experiment steps for the MB labeled target sequence. The Bare gold surface was modified with a thiolated probe using thiol-on-gold self-assembled monolayer. Hybridization state for MB modified complementary (a) and non-complementary target (b) state was demonstrated.

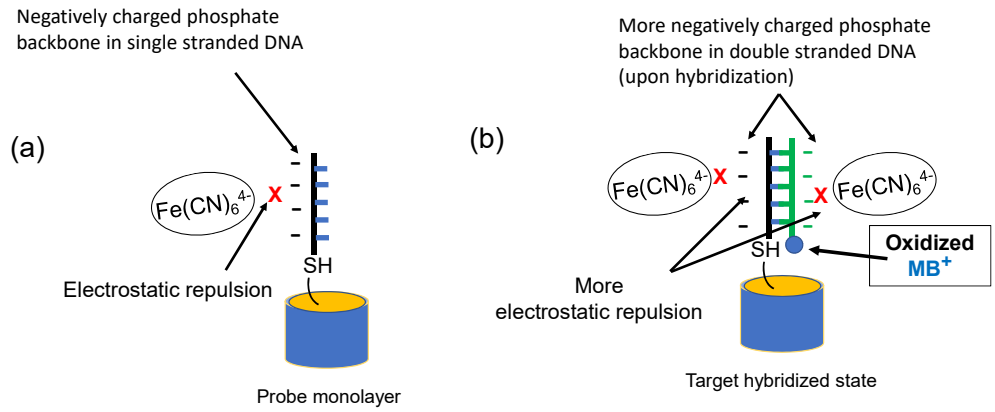

Figure 3.6: Schematic demonstrates the electrostatic repulsion between negatively DNA phosphate backbone and negativity charged Ferrocyanide before (a) and after hybridization of MB-tagged target (b).

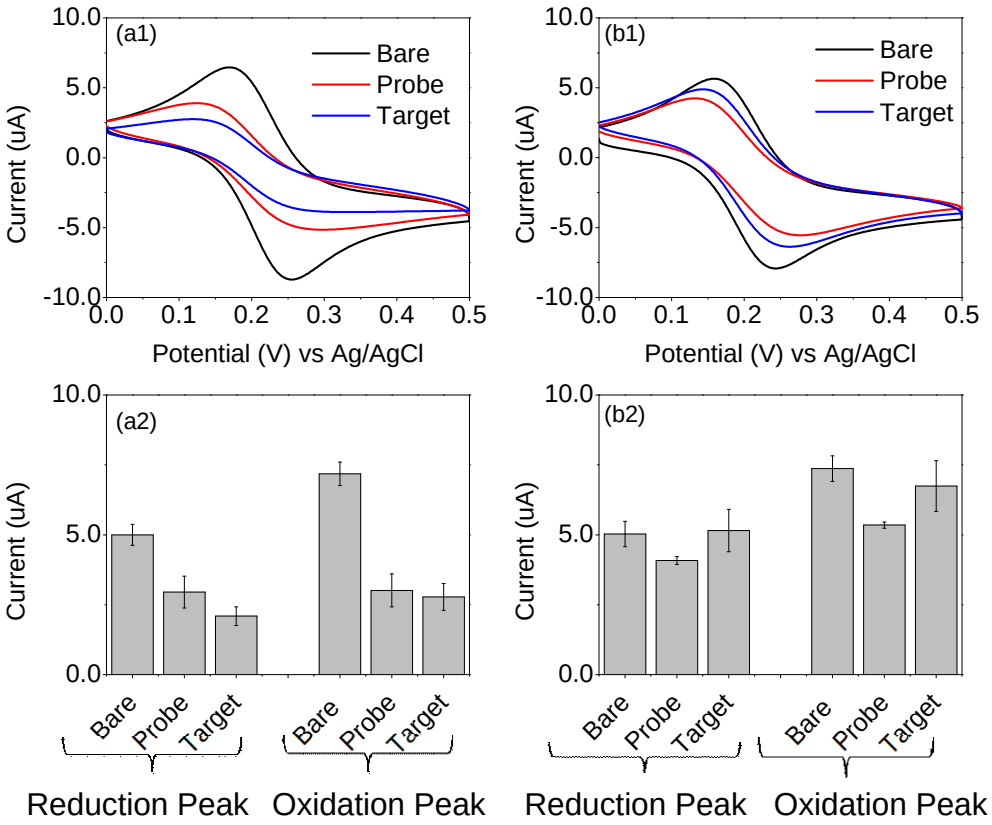

Figure 3.7: a1 and b1 are the Representative cyclic voltammogram, a2 and b2 are the oxidation and reduction peak for complementary and non-complementary targets respectively, for Bare, Probe-MCH monolayer and the Target hybridization state for MB labeled target. Hybridization was performed with (a)1 μM complementary target, L2 and (b)1 uM noncomplementary target, L3. CV was performed in 25 mM PB solution, 25 mM NaCl and 2 mM $[Fe(CN)_6]^{4-}$ with scan setting shown in section 2.2. Error bars show a Standard error for the 3 trials.

Table 3.2: Peak reduction/oxidation current and voltage for the **MB** labeled complementary and non-complementary target modification on the sensor surface

Complementary Target	Bare	Probe	Hybridized state
Reduction Current, I_{PC}	6.45 μA	3.8 μA	2.64 μA
Oxidation Current, I_{Pa}	8.706 μA	5.07 μA	5.07 μA
Reduction Voltage, E_{PC}	0.172 V	0.142 V	0.143 V
Oxidation Voltage, E_{Pa}	0.257 V	0.273 V	0.265 V
Peak to Peak separation, E_{p-p}	0.081 V	0.189 V	0.214 V
Non-Complementary Target	**Bare**	**Probe**	**Un-hybridized state**
Reduction Current, I_{PC}	5.611 μA	4.164 μA	4.792 μA
Oxidation Current, I_{Pa}	7.91 μA	5.507 μA	6.349 μA
Reduction Voltage, E_{PC}	0.165 V	0.145 v	0.156 V
Oxidation Voltage, E_{Pa}	0.240 V	0.260 v	0.256 V
Peak to Peak separation, E_{p-p}	0.075 V	0.115 V	0.004 V

3.3 Voltammetry technique

The electrochemical signal was measured in 25 mM PB solution and 25 mM NaCl for a comparative study of widely used voltammetry techniques; DPV, SWV, and ACV. Surface modification for this experiment is illustrated in Figure 3.6; the bare gold surface was modified with a thiolated probe using thiol-on-gold self-assembled monolayer. Target and probe signal was analyzed for the hybridization of MB modified complementary target. Since the target is redox labeled, we eliminate the redox species in the scan solution. This system will enable us to see MB redox signal only after the hybridization. Reduction reaction of MB is shown in Figure 1.11-B.

A planar bare gold electrode was modified with the single-stranded thiolated probe using the thiol-on-gold self-assembled monolayer (Figure 3.8). The sensor was challenged with an MB tagged complementary target. Since electrochemical signal was taken in the buffer solution, no signal is expected in the probe measurement, and it is expected to see a well defined MB reduction current with a sharp peak at around -0.3 V indicating MB redox reaction.

Sample DPV, SWV, and ACV scans were demonstrated in Figure 3.9. Peak current study represented in the bar graph directed us to choose SWV, which shows the highest peak current of about 2 uA with comparably lower standard deviation with respects to the DPV and ACV).

Table-3.3 listed the acquisition time for each scan for the typical pulsed voltammetry techniques studied in this section, which indicates 30 seconds for the DPV, 9 seconds for the SWV and 10 minutes for obtaining a single voltammetry measurement was required to achieve per scan. Acquisition time for SWV is 9 seconds, which is lowest among the pulse voltammetry techniques studied (Table 3.3). Previous studies in the literature

also support our findings [52] that states; square wave voltammetry can be used to experiment much faster than differential pulse techniques, which typically run at scan rates of 1 to 10 mV/sec. Square wave voltammetry employs scan rates up to 1 V/sec or faster, allowing much faster determinations.

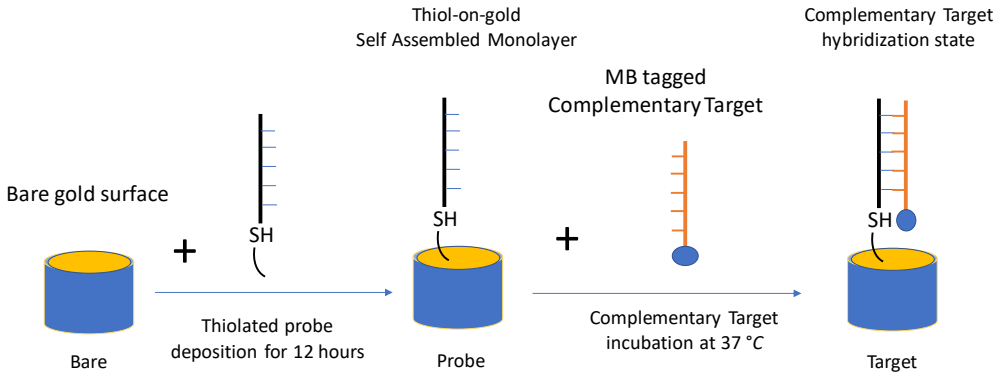

FIGURE 3.8: Schematic demonstrates the hybridization experiment steps for the MB labeled target sequence. The Bare gold surface was modified with a thiolated probe using thiol-on-gold self-assembled monolayer. Hybridization state for MB modified complementary.

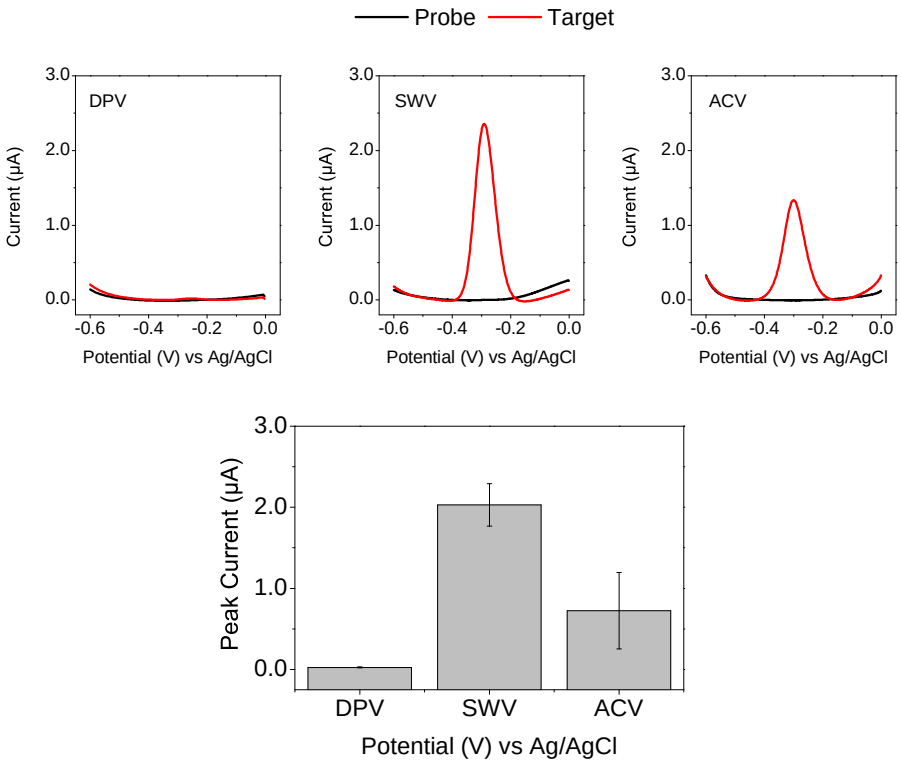

Figure 3.9: Top row shows sample DPV, SWV, and ACV for representative probe and target hybridization. The bar graph shows peak target current analysis for these voltammetry techniques. Standard error bars are shown.

Table 3.3: Time required for the different Pulse voltammetry techniques.

Voltammetric Technique	Time required to acquire each scan
DPV	30 Seconds
SWV	9 Seconds
ACV	10 Minutes

3.4 Scanning solution determination for signal enhancement

To determine a scanning solution that gives the largest signal change, hybridization experiment for MB-labeled target were performed in $[Fe(CN)_6]^{3-}$ (25 mM PB solution, 25 mM NaCl and 0.25 mM) and buffer solutions (25 mM PB solution and 25 mM NaCl) using SWV. The percent change from probe signal to target signal peak was analyzed. Figure 3.10 below shows a comparative study of this experiment. Although the experiment was performed with three electrodes for each target sequence, data for only one electrode is shown in each graph for the sake of visual clarity. Figure 3.11 shows schematic percent change calculation protocol for this experiment.

Upon hybridizing 1 μM MB-tagged complementary target L2, $[Fe(CN)_6]^{3-}$ system shows 1.5×10^2 times increase to the probe signal (Figure 3.10-y). In this experiment both MB (tagged with target) and $[Fe(CN)_6]^{3-}$ present in the solution and both get reduced at the same potential (-0.3 V). Signal enhancement for the target is due to the collective reduction of MB and $[Fe(CN)_6]^{3-}$ at the same potential (for 10 nM and 1 μM complementary target). However, for the lower target concentration, 1 pM and 100 pM a lower SWV peak is observed. Which is an unusual behavior according to the hypothesis stated above. To explain such unusual behavior further investigation is required.

For the buffer system (Figure 3.10, x), since the target is modified with MB redox reporter, eliminating the redox agent in the scan solution ($[Fe(CN)_6]^{3-}$) gives a negligible background signal compare to the MB redox peak for the target. Probe to target signal change is also calculated to show comparative study with the $[Fe(CN)_6]^{3-}$ system. Since there is no peak observed due to the absence of the redox agent in the scan solution, probe current corresponding to the target peak was taken to calculate the signal change. Protocol for the calculation schematically demonstrated in the in Figure

3.11 for each case. In the buffer system, for 1 μM target, 1.2 $\times$ 10^5 % signal change was observed (Figure 3.10-x) compared to the 1.4 $\times$ 10^2 % signal change for 1 μM target in $[Fe(CN)_6]^{3-}$ system (Figure 3.10-y). This system shows detectable signal up to 1 pM target concentration. The advantage of the buffer system over the $[Fe(CN)_6]^{3-}$ system is that, since there is no peak observed for the probe solution, it is possible to directly compare the target signal peak with the blank signal to determine the detection limit of the PRPDA system.

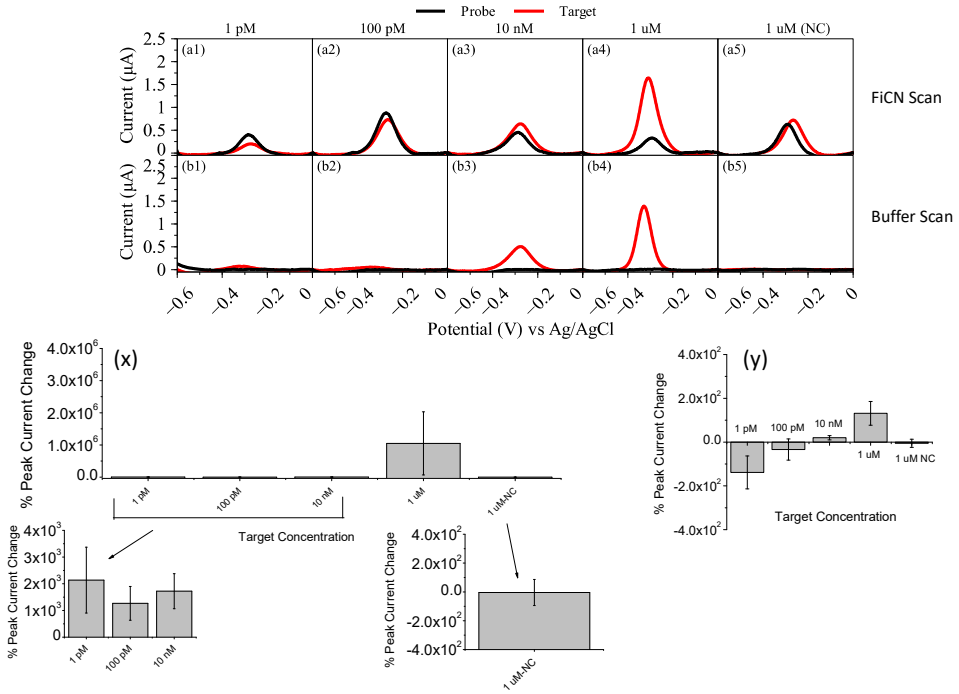

FIGURE 3.10: Top row shows sample SWV for the experiment in $[Fe(CN)_6]^{3-}$ (a1-a5) and buffer solution (b1-b5) for the target concentration from 1 pM, 100 pM, 10 nM, 1 uM complementary and 1 uM non-complementary. x and y shows the percent peak current change from the probe to target vs. varying target concentration for buffer and $[Fe(CN)_6]^{3-}$ solution consecutively.

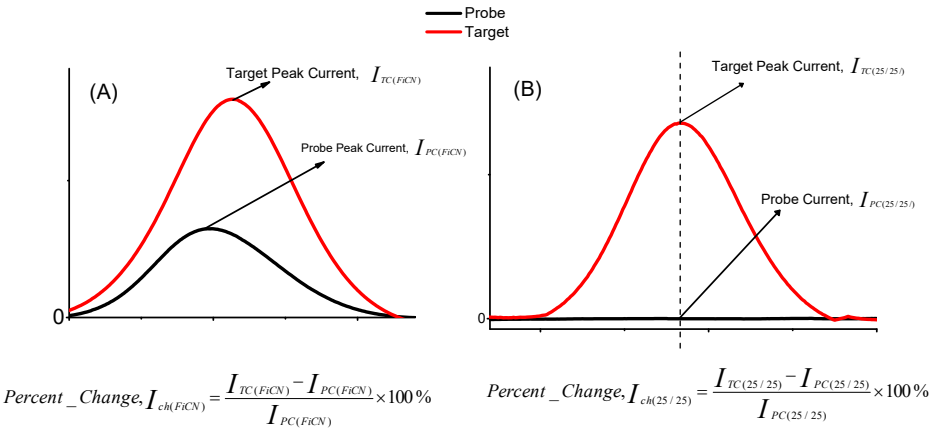

FIGURE 3.11: Schemetic showing the percent change calculation for $[Fe(CN)_6]^{3-}$ system (A) and the Buffer (25/25) (B) system.

3.5 Strand displacement assay

In this section, we demonstrate the detection of redox-labeled DNA sequences using electrochemical readout through toehold-mediated strand displacement assay, which is a key step for signal generation in the PRPDA protein detection system. Figure 3.12 demonstrates the toehold-mediated strand displacement reaction. In toehold-mediated strand displacement reactions, a single-stranded domain first binds to the dangling toehold domain of a pre-hybridized double-strand. This triggers the branch migration and results in the dissociation of the strand previously bound to the substrate. The toehold domain plays an important role in facilitating strand displacement, and the length of toehold is often used to control its reaction kinetics [53].

To develop an electrochemical biosensor based on PRPDA, planar gold electrodes were modified with a thiolated duplex probe carrying a toehold. Upon introduction of methylene blue (MB) modified target, a toehold mediated DNA displacement process is initiated. Square Wave Voltammetry (SWV) was performed in a buffer solution to analyze the electrochemical signal change before and after hybridization. We studied system's hybridization kinetics and limit-of-detection by documenting the hybridization-induced changes in the SWV signal.

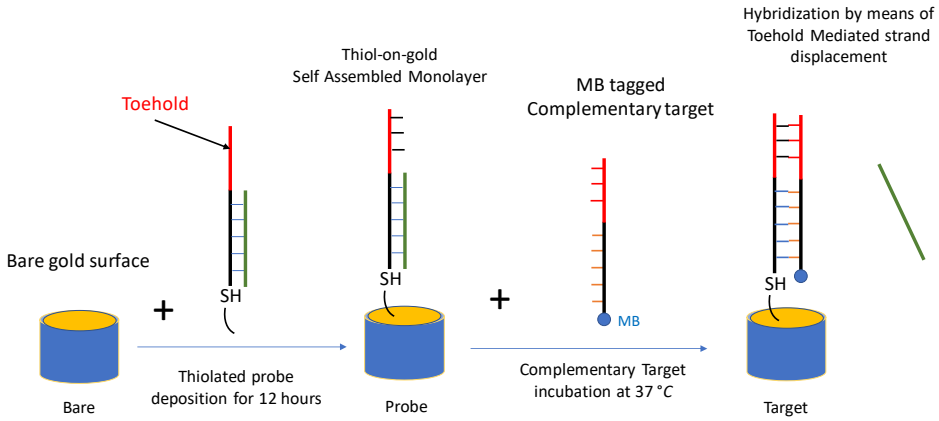

FIGURE 3.12: Schematic showing toehold-mediated strand displacement process. A bare gold surface is modified with a thiolated pre-hybridized capture probe, then the capture probe challenged with the MB tagged complementary target. The strand displacement reaction initiated by binding with a complementary sequence to the toehold in the target oligo. Hybridization process ended up by displacing the protected sequence (shown in green color) from the prehybridized state.

3.5.1 Hybridization Kinetics of DNA strand displacement

We studied time depended hybridization kinetics of the proposed toehold mediated DNA strand displacement assay demonstrated in section 3.5. As shown in figure 3.12, the target sequence binds to the toehold to the prehybridized (protected) capture probe (CP) and displaces the protection probe (green color in Figure 3.12) to hybridize with the immobilized (on gold) strand. The purpose of this experiment is to determine the optimum hybridization time that shows highest signal compare to the blank for the toehold-mediated strand displacement assay.

In this study, 1 μM of the prehybridized capture probe, CP, containing a toehold, was immobilized on the planar gold surface. Then, 10 nM of MB tagged; complementary target sequence, L2, and non-complementary target sequence, L3 were introduced for 2 min, 30 min, 2 hours, 4 hours, 14 hours, and 24 hours. After the hybridization of complementary target, L2, MB is expected to come to the proximity to the gold surface and reduction of MB was recorded by SWV.

Figure 3.13 presents the peak current vs. hybridization time recorded for 2 min, 30 min, 2 hours, 4 hours, 14 hours, and 24 hours. It is evident from the Figure 3.13 that though the highest target peak current was observed between 14 hours and 24 hours, 2 hours is the lowest incubation time when a detectable signal for the target is visible. Upon introduction to the non-complementary target, for 24 hours, a small SWV was observed. We don't expect to see an MB reduction peak when non-complementary sequence, L3, was introduced. The straight line shows the background signal upon non-complementary target introduction for 24 hours incubation time. We hypothesize that this small background current is due to MB-gold nonspecific adsorption. A detailed study was performed to address this non-specific adsorption and unwanted hybridization, and the study is reported later in section 3.6.

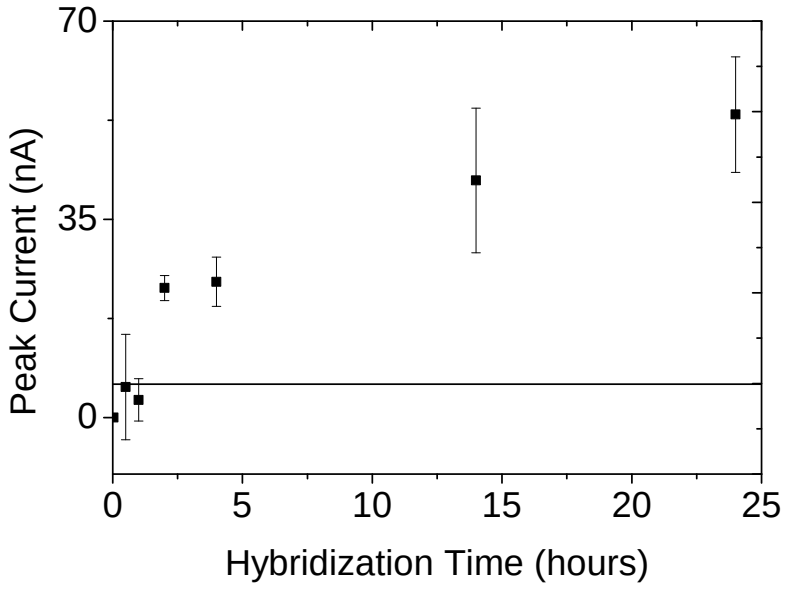

Figure 3.13: Average peak current vs. Hybridization time for 10 nM complementary target (average taken for 3 trials). Error bar represents Standard Deviation (SD) from the mean. The straight line represents the SD of 10 nM non-complementary target.Time recorded for 2 min, 30 min, 2 hours, 4 hours, 14 hours, and 24 hours.

3.5.2 Limit of detection (LOD) for strand displacement assay

We performed a Limit of Detection (LOD) experiment for the strand displacement assay developed in this section. The planar electrode was modified with the thiolated pre-hybridized capture probe and challenged with the complementary target, L2, with the concentration of 1 pM, 100 pM, 10 nM and 1 uM. To gauge the background signal, 1 μM of the non-complementary target was introduced. Determined from the kinetics experiment in section 3.4.1, 2 hours incubation time was chosen for the hybridization reaction to take place. The limit of detection experiment characterizes the lowest amount of complementary target DNA which can be detected and distinguished from non-complementary target DNA. LOD is calculated as $\pm 1SD$ of the complementary target peak current ($I_{(p-c)}$) is greater/equal to the $\pm 3SD$ of non-complementary target (background signal) peak current ($I_{(p-nc)}$), which can be mathematically expressed as: $LOD = I_{(p-c)} \pm 1SD \geq I_{(p-nc)} \pm 3SD$.

Figure 3.14(top) shows sample Square Wave Voltammogram before (probe) and after the capture probe (CP) challenged with the complementary target with a concentration of 1 pM, 100 pM 10 nM and 1 μM. Figure 3.14 (bottom) demonstrates average peak current vs. target DNA concentration that recorded form a triplicate experiment for each concentration. LOD was calculated to be 10 pM for the strand displacement assay. ($I_{(p-c(100pM))} \pm 1SD = 4.28nA > 2.9nA = I_{(p-nc(10nM))} + 3SD$). However, detectable signal up to 1 pM was observed. Which is an indication that LOD can be further reduced by optimizing the assay for PRPDA.

In this work, we have successfully demonstrated that hybridization of MB-modified complementary DNA can be detected electrochemically by toehold-mediated strand displacement. LOD of 100 pM with a detectable signal up to 1 pM was demonstrated. We expect to increase the sensitivity and limit-of-detection of this system by employing high

surface area wrinkled gold electrodes. We will further use this system for the detection of protein biomarkers using the proposed target-responsive dynamic DNA assembly.

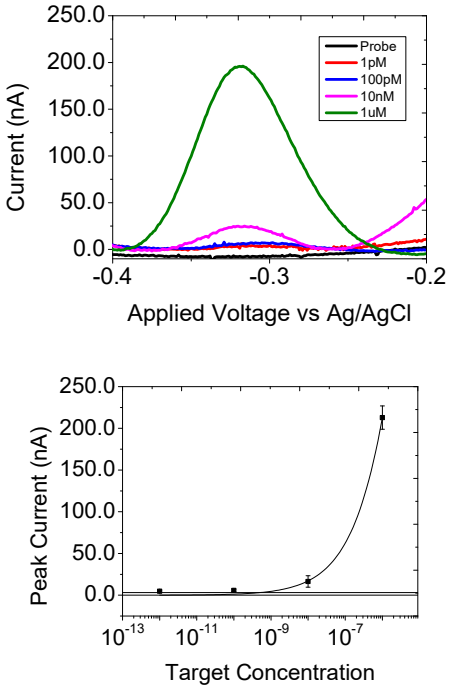

Figure 3.14: Sample Square Wave Voltammetry signal before (Top) and after hybridization (Bottom). Probe signal shows no redox peak. Scans after hybridization with 1 pM, 100 pM, 10 nM and 1 μM complementary target solutions show the methylene blue redox signal in 25 mM NaCl and 25 mM PB solution. Average peak current versus target DNA concentration shown in the right graph. Average taken from 3 successful trials for 1 pM, 100 pM, 10 nM and 1 uM complementary targets and 1 μM non-complementary target. Error bars represent the standard deviation from the mean. The straight line represents the 1 SD of 1 μM non-complementary target.

3.6 Reducing the blank signal level

As seen figure 3.1, a large unexpected background signal present in the blank. We hypothesize that this could be due to two reason; 1) Non-specific adsorption of MB-gold, 2) Unwanted hybridizationdue to target independent three way junction formation.The goal of this experiment is to reduce the background signal present due to unwanted hybridization and nonspecific adsorption in the PRPDA system by simulating the final step of the experiment. In the PRPDA assay, which involves protein in the system, a single-stranded MB tagged reporter (named as ss-MB for this experiment) probe is released. In the absence of a protein target, the reporter probe is in a protected state, which is called a ds-MB in this experiment. ss-MB and ds-MB simulate target and controlled state, respectively for the PRPDA system. For the visual clarity, a schematic of ss-MB and ds-MB sequence used here presented in the Figure 3.16.

To assess the background signal generated in the absence of the protein target, the following experiment was performed; 1) The duplex was formed in the controlled environment inside the thermal cycler. 2) After immobilizing the duplex capture probe, it was challenged with a protection probe to make sure no single-stranded oligonucleotide is present. 3) Duplex and MB (control and target reporter probe respectively in the PRPDS assay) were further diluted and 4) finally an additional surface blocker is introduced to the target solution to avoid MB-gold affinity binding. The outcome of each experiment is presented in the figure 3.17 discussed below.

In the initial experiments, prehybridized duplex reporter probe ds-MB (Figure 3.16 top schematic) and Capture probe were prepared by cooling down the solution by placing them in open air followed by heating at 95 °C. An experiment was performed by modifying the cool down protocol to the controlled environment in the thermal cycler with 5 °C temperature increments in 2 min time intervals down to room temperature.

Figure 3.17-(1) demonstrates Peak SWV current recorded before and after controlled temperature protocol employed. Signal (ss-MB) to noise (ds-MB) ratio was compared the before and after optimization condition. After the controlled temperature protocol employed, MB-labeled target shows a 187.45 % signal (ss-MB) to the noise (ds-MB) ratio compared to the 54.68 % calculated for the uncontrolled protocol. These unprotected single-stranded capture probes on the gold sensor surface could reversely displace the protected strand from the ds-MB target separating the single-stranded MB target and hybridize with the capture probe leading to a false positive signal. By employing the controlled protocol to form prehybridized duplex, it is possible to reduce the number of prehybridize capture probe on the sensor surface.

The next experiment was done by further introducing the protected probe (shown in schematic in figure 3.16) on the sensor to block if any unprotected probe remains, which may reversely displace the MB from the duplex reporter probe, which shows (figure 3.17 (2)) about 15. 97 % decrement of signal to noise ratio. Before introducing the post protection probe, there was 54.68 % increment in signal to noise ratio The decrement of target signal for MB labeled target (ss-MB) after introducing the post protection probe is not supported by our hypothesis and still to be understood and require further study.

Next, an experiment was performed by diluting the target sequence 100 times. We hypothesized that by diluting further the ss-MB and ds-MB, it would be less thermodynamically favorable for the MB to electrostatically attach to the gold surface. But by showing a decrease of 16.79% in the peak current for the ss-MB target compare to the ds-MB target, this experiment failed to support our hypothesis. Results of this experiment is presented in Figure 3.17 (3).

Next, we proposed to introduce poly-A oligonucleotide sequence with 17 nucleotide to the target solution (ss-MB and ds-MB). Poly-A is negatively charged in neutral pH, and adenine has an affinity for the gold surface [54]. When sensor is challenged with the

target sequence that mixed with the Poly-A, due to the strong non-affinity energy to the gold compare to the MB [55], Poly-A horizontally attached on the gold electrode surface, inhibiting the nonspecific binding of the MB on the gold surface. We demonstrated the hypothesis with a schematic in Figure 3.19. Poly C nucleotide also demonstrates strong affinity with different electrode materials, but the affinity of Poly-A was found to be stronger with gold compared to Poly-C [55]. The results of introducing 10 nM poly-A shows (Figure 3.17-(4)) larger signal to noise ration of 63.99 % which is small improvement compared to the 54.48 % without poly-A in the target solution. Although this difference is small, we expect to increase the signal to noise ratio by further optimization of Poly-A concentration.

This experiment suggests that by preparing the duplex probes in the controlled temperature protocol and introducing the poly-A in the target solution, it is possible to reduce the nonspecific adsorption and unwanted hybridization. We proposed an experiment to study the role of concentration variation of poly-A sequence on the signal to noise ratio.

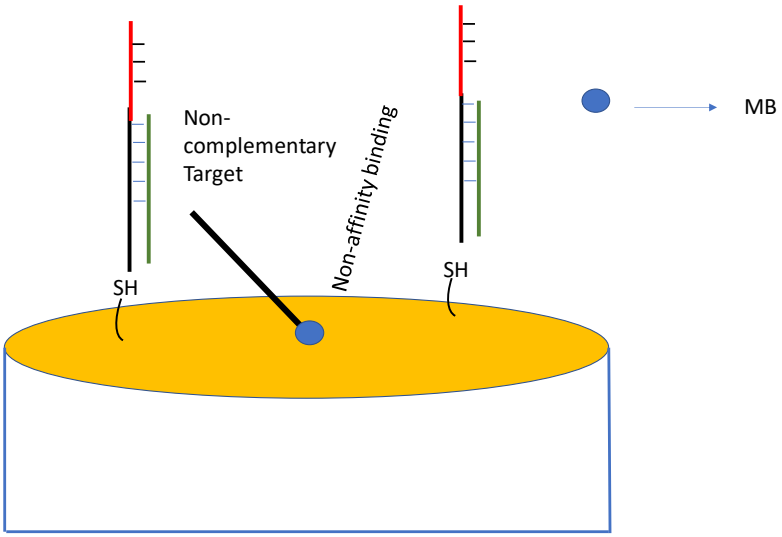

Figure 3.15: Schematic showing the hypothesis for nonspecific adsorption take places due to non-affinity binding between MB and Au electrode surface

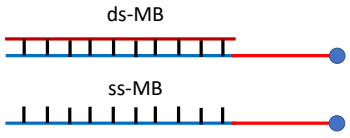

Figure 3.16: Schematic for the target sequence designed for blank signal reduction experiment. ds-MB is the pre-hybridized state of the reporter probe. ss-MB is the single-stranded MB redox tagged target oligo sequence.

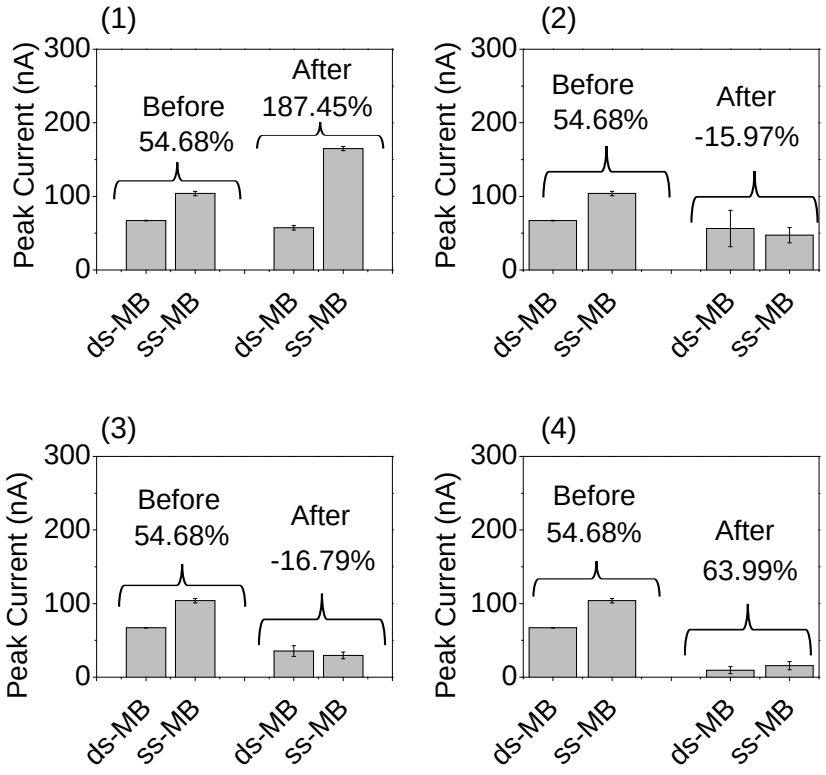

Figure 3.17: Nonspecific adsorption optimization by (1) Controlled temperature protocol for probe protection, (2) extra protection the probe on the sensor, (3) Dilution of the reporter probe, (4) With Poly A in the target solution as an extra surface blocker.

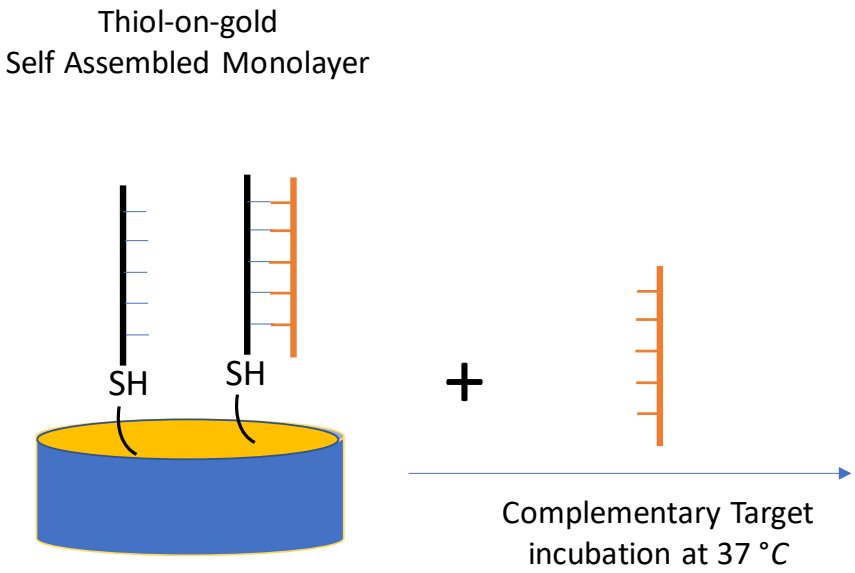

Figure 3.18: Schematic showing post hybridization protocol.

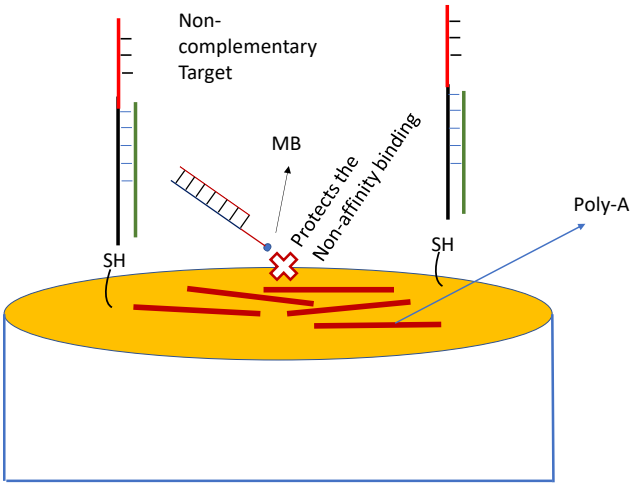

FIGURE 3.19: Schematic showing that Poly-A non-affinity binding on the gold electrode surface inhibits the nonspecific adsorption of MB on the gold.

3.6.1 Poly A concentration optimization

The experiment presented in the previous section suggests that introducing poly -A helps to reduce the nonspecific adsorption of ds-MB on the gold surface. We performed an experiment varying the Poly-A concentration to observe its potential in reducing the nonspecific adsorption further. Signal to noise ration of target solution contained Poly-A concentrations of 10 nM, 100 nM, 1 μM and no poly-A was analyzed. The results in Figure 3.20 suggest that with 1 μM poly-A in the target solution, the highest reduction in nonspecific adsorption is observed (with a signal to noise ratio of 4900%). It is worth to mention that the signal to noise ratio for the poly-A concentration of 0 to 1 μM pol-A does not follow a particular trend. More experiment is required to understand and explain the relationship between the poly-A concentration and signal to noise ratio.

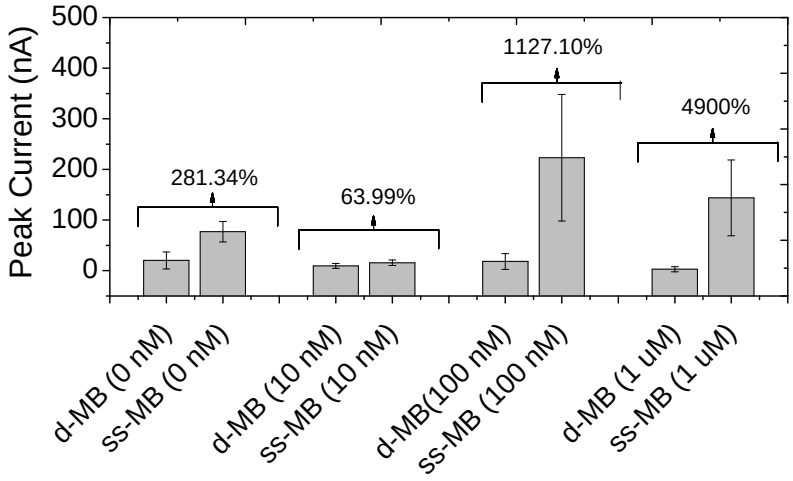

Figure 3.20: Peak current vs Poly A concentration (in bracket) for ss-MB target versus ds-MB control. Poly A concentration of 10 nM, 100 nM, 1 uM and without Poly A was examined for ds-MB vs ss-MB. Percent change from control to MB peak current is indicated on each bar graph

3.6.2 Intermediate sequence optimization

The study published by Li et al [1] that employs fluorescence readout with a similar assay, demonstrated that concentration of intermediate sequence TB=B*C in the PRPDA assay (Figure 1.11-A). (Intermediate sequence TB=B*C in PRPDA electrochemical based assay is indicated in Figure 3.21) is critical for manipulating the the kinetics of the formation of three-way junction (TWJ) that allows releasing the fluorescent tagged reporter probe in the absence of the protein target. In our design, we suspect that the TB=B*C concentration is high enough to facilitate the formation of TWJ in the absence of protein target allowing the release of the redox tagged reporter probe showing the background signal.

In the effort to optimize the false positive signal involved in the formation TWJ in the absence of protein target, we systematically reduced the concentration of the TB=B*C sequence. TB=B*C concentration of 12.5 nM, 25 nM and 50 nM were chosen. A percent change in the average peak current of the target to blank was calculated to analyze the background signal optimization.

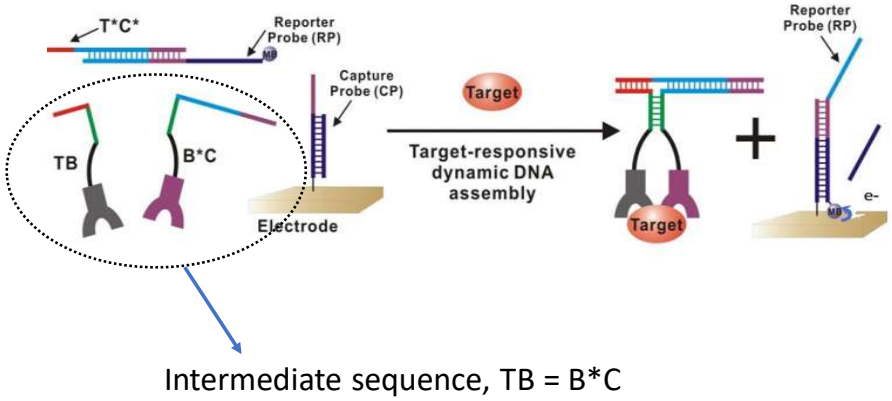

Figure 3.21: Schematic of proposed model indicating the intermediate sequence TB=B*C sequence

It is evidence from figure 3.22 that, in the absence of protein target (Blank) in the PRPDA assay, average peak current decreases (shown with an arrow) with the decrease of TB=BC concentration. Which indicates that the TWJ formation is less thermodynamically favorable for the lower TB=BC concentration. The percent peak current change for target to the blank shows difference ratio of 288.98% for the 12.5 nM TB=B*C, compare to the 75.03% for 25 nM and 124.04% for the 50 nM respectively. Though target average peak current does not vary significantly with the decrease of the TB=B*C concentration, a larger standard deviation (SD) was seen for the lower TB=B*C concentration. Due to a higher signal to noise ratio we chose the TB=B*C concentration of 12.5 nM for the detection limit experiment.

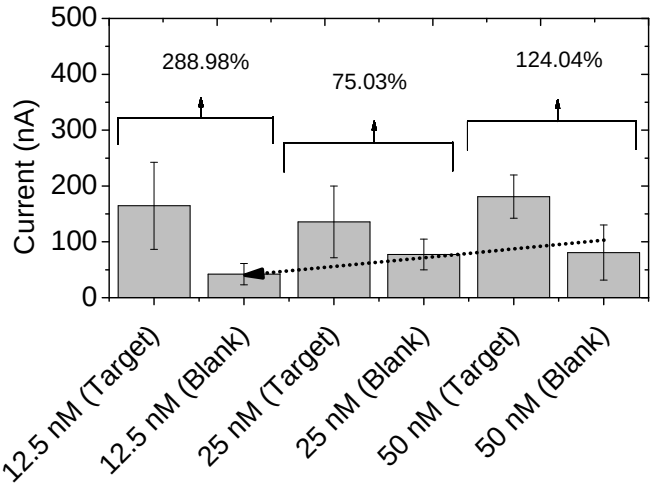

Figure 3.22: Peak current vs TB=B*C concentration of 12.5 nM, 25 nM and 50 nM. Error bar shows standard deviation from the mean.

3.6.3 Time-dependent kinetics study of the PRPDA assay

Li et al. shows that, the target independent three-way junction (TWJ) formation to release the reporter probe (Figure 1.10) is time-dependent. For the longer incubation higher background signal for the PRPDA system was observed in the florescence assay [1]. To determine the kinetics for unwanted hybridization due to target independent TWJ formation and compare signal to noise ratio, the incubation time of 2 hrs.,1 hr. And 30 min was chosen.

Data shown in figure 3.23 is presented with the average peak current for the target and blank for 30 min, 1hr and 2 hr incubation time. Blank signal shows an increase in the average peak current which is in line with the hypothesis presented by Li et al. that, with the increase of incubation time, the formation of toehold mediated TWJ in more thermodynamically favorable to release more redox tagged reporter probe. For the 30 min incubation highest signal to noise ratio of 369.45% was observed compared to the 175.66% for the 1 hr and 261.98% for the 2 hr incubation time. This experiment is the evidence that for the 30 min incubation PRPDA shows highest signal to noise ratio.

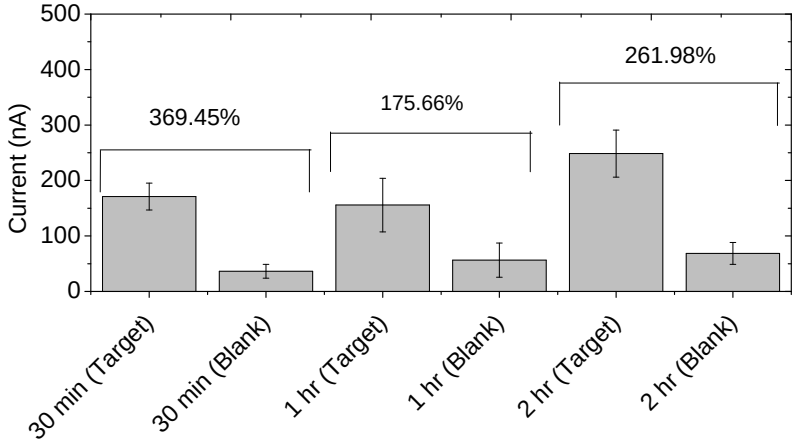

Figure 3.23: Peak current vs. incubation time of 30 min, 1 hr and 2 hr in the presence (target) and absence (blank) of protein in PRPDA scheme. Error bar shows standard deviation from the mean.

3.7 LOD on planar and wrinkled electrodes

It has been shown in previous studies that the limit of detection of the biomolecular sensor strongly depends on the nanoscale texturing of the electrode surface [35, 56–59] Gabardo et al. demonstrated that increased surface area of the porous nanostructure electrodes enhances sensitivity in the DNA hybridization detection compared to the flat surface by enhancing the accessibility during the hybridization reaction requiring shorter hybridization time [60].Here we performed a limit of detection experiment to study the sensitivity of the PRPDS protein detection assay (section 1.5) on and porous gold electrodes.

To perform the LOD experiment, a set of three electrodes for both planar and porous surfaces were prepared following the electrode preparation protocol described in the section 2. The surface of the electrodes was modified with the pre-protected capture probe that carries a toehold (protocol explained in section 2.2). Protected reporter probe (TC:C*-MB) concentration of 10 nM, Intermediate sequence, TB=B*C concentration of, 12.5 nM (section) was chosen based on the experiment performed in the previous section. The peak current density for the electrochemical SWV was recorded for the target concentration of 1 fM to 1 μM. Sample SWV for PRPDA protein detection assay performed for different target concentration in both planar and wrinkled gold electrode is shown in Figure 3.24 with the log linear change of peak current density vs concentration. For the comparative study, date are represented in terms of current density.

LOD calculated with the same algorithm explained in section 3.5.3. That LOD is the concentration at which the current density of target, $J_{target} \pm 1SD$ is greater/equal to, current density of blank, $J_{blank} \pm 3SD$, which can be expressed as; $LOD_{PRPDS} = J_{target} \pm 1SD \geq J_{blnak} \pm 3SD$. For the planar electrode, for 10 pM target, $J_{target} \pm 1SD = 2.05 \times 10^{-6} \pm 7.07 \times 10^{-7} = 2.75 \times 10^{-6}, 1.34 \times 10^{-6}$, which is the lowest

target concentration that have, $J_{target} \pm 1SD$ greater then the current density for blank, $J_{blnak} \pm 3SD = 3.43 \times 10^{-7} \pm 2.16 \times 10^{-8} = 2.50 \times 10^{-6}, -1.82 \times 10^{-6}$. Hence, LOD for the planar electrode was determined to be 10 pM. For the wrinkled electrode, for the 1 pM target, $J_{target} \pm 3SD = 3.78 \times 10^{-6} \pm 3 \times 1.06 \times 10^{-7} = 4.10 \times 10^{-6}, 3.46 \times 10^{-6}$, which is the lowest target concentration that have, $J_{target} \pm 1SD$ greater then the, $J_{blnak} \pm 3SD = 2.16 \times 10^{-6} \pm 1.90 \times 10^{-6} = 4.06 \times 10^{-6}, -2.6 \times 10^{-7}$. Hence, LOD for the wrinkled electrode was determined to be 1 pM, which is ten times greater compare to the planar electrode. This is in line with the hypothesis reported by the Gabardo et. al. [60] that increased electroactive surface area improves the sensitivity of the sensor.

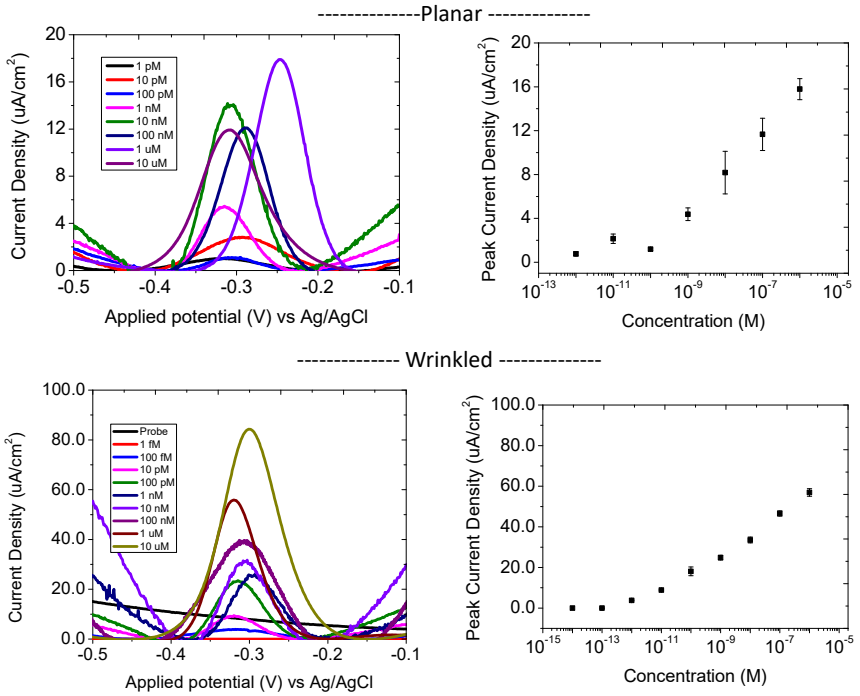

Figure 3.24: Top left, representative Square Wave voltammogram of PRPDA assay performed on planar electrode for target protein concentration from 1 pM, 10 pM, 100 pM, 1 nM, 10 nM, 100 nM and 1 μM. Current represented in current density. Top right shows peak current density vs log-concentration for the experiment performed on planar gold electrode. Bottom left, representative Square Wave voltammogram of PRPDA assay performed on wrinkled electrode for target protein concentration from 1fM, 100 fM, 1 pM, 10 pM, 100 pM, 1 nM, 10 nM, 100 nM and 1 μM. Current represented in current density. Top right shows peak current density vs log-concentration for the experiment performed on wrinkled gold electrode.

3.8 Summary

In this chapter, in section 3.2, we presented the characterization of the DNA hybridization sensor modification on the planar gold electrode surface for the label-free and labeled (MB tagged) target DNA detection. Cyclic voltammetry (CV) was used to differentiate the redox reaction of $[Fe(CN)_6]^{3-}$ on the bare gold electrode, probe modification, and target hybridization state. Well defined $[Fe(CN)_6]^{3-}$ reduction/oxidation peak current decrement in CV from the bare gold electrode to probe monolayer modification and target hybridization state was the indication of the successful development of hybridization sensor using electrochemical readout. The decrease in the reduction/oxidation peak current is due to repulsive electrostatic interactions between the anionic $[Fe(CN)_6]^{3-}$ redox marker and the polyanionic P1 probes (negatively charged phosphate groups of the DNA backbone) as well as DNA/MCH monolayer, which act as a physical blocking layer, fewer faradic processes take place with slower reaction kinetics [48].

In section 3.3, we presented a comparative study of the major voltammetry techniques, Differential pulse voltammetry (DPV), Square Wave voltammetry (SWV) and Alternative current voltammetry (ACV). The experimental result suggests that SWV provides a higher peak compare to the DPV and ACV techniques with the lowest time require per scan.

In section 3.4, we compared the use of $[Fe(CN)_6]^{3-}$ and Buffer only solutions to determine the scan solution providing the largest signal change for the target to probe for the target concentration of 1 uM to 1 pM. The percent peak current change for the target to probe calculated for $[Fe(CN)_6]^{3-}$ system vs buffer system was analyzed, showing a detectable percent peak current change up to 1 pM for the buffer only system with a inconsistent trend for the target concentration change . This experiment suggested using the buffer only solution as the scan solution for the later experiments.

In section 3.4, we present the development of the toehold mediated strand displacement assay that is an essential reaction for the PRPDS protein detection scheme. Time-dependent hybridization kinetics and a Limit of Detection (LOD) study was carried out for the toe-hold mediated strand displacement assay. This experiment indicates a after 2 hours incubation no statistically significant improvement of the signal have observed and a detectable signal up to 1 pM with a LOD of 10 nM. We further used this system for the detection of protein biomarkers using the proposed target-responsive dynamic DNA assembly and high surface area wrinkled gold electrodes.

Section 3.5 was presented with the study performed to increase the ssDNA to ds-DNA current ratio. To do so, we prepared the duplexes in the controlled environment in the thermal cycler, introduced post-hybridization protection strands on the sensor and finally introduced negatively charged poly-A to the target solution for its stronger affinity with the gold electrode compared to the MB. This experiment suggests that by employing controlled temperatures to form a duplex and introducing poly-A helps increase the ssDNA to dsDNA current ratio. We then performed an experiment varying poly-A concentration to determine the concentration of poly-A at which sensor gives the highest ssDNA to dsDNA current ratio. This experiment suggests that introducing 1 uM poly to the target solution provides the ssDNA to dsDNA current ratio. Next, an experiment was performed varying concentration of intermediate sequence (TB=B*C) and the incubation time of the PRPDS assay that suggests at 12.5 nM TB=B*C concentration for 30 min incubation gives the highest target to blank peak current ratio for the 10 nM protein target.

Finally, we performed the Limit of Detection (LOD) study for the PRPDS system choosing the 12.5 nM of intermediate sequence, TB:B*C , 10 nM protected reporter probe TC:C*-MB and 30 min incubation time suggested by the optimization experiments that showed the highest target to blank peak signal ratio. Both planar and porous

wrinkled gold electrodes were modified with CP:P* duplex capture probe. Protein target concentration from 1fM to 10 uM was used with a 10 times dilution to challenge the PRPDS assay introducing 1 uM poly A in the target solution. LOD for the planar electrodes and wrinkled electrodes were calculated to be 10 pM and 1 pM respectively. 10 $\times$ improvement in the LOD for the porous wrinkled gold electrodes suggests the hypothesis presented by Gabardo et. al [60] that nonporous gold electrodes increase the electroactive surface area and the sensor sentivity

Chapter 4

Conclusions

4.1 Contribution to the field

Major contribution of this thesis is the improvement of the limit of detection (LOD) of existing protein sensor development based on the protein responsive programmable dynamic DNA assembly (PRPDA) [1]. Specifically, my research focuses to introduce electrochemical readout to the improve LOD on previously reported fluorescence readout to develop PRPDA scheme. We have reduced the limit of detection of the fluorescence assay from 2.8 nM to 1 pM.

My work identifies that signal to noise ration of the sensor decreases due to two reason; 1. Non-affinity binding between redox reporter, MB and gold electrodes and 2. Unwanted hybridization due to target independent three way junction (TWJ) formation. This can be improve by introducing poly-A to the target solution. Due to higher affinity of poly-A to gold compare to MB, poly-A strongly binds to the gold surface allowing to wash unbound MB easily. We further demonstrated that an optimum incubation time that provides an enhanced signal to noise ratio. Finally, we have demonstrated that by employing high surface area wrinkled gold electrode, LOD up to 1 pM is achievable which is ten-fold higher compare to 10 pM calculated for the planar gold area. 1 pM

LOD for PRPDA system is a significant improvement over 2.8 nM LOD reported for fluorescence transduction.

4.2 Thesis summary and conclusion

Chapter 1 discusses the proposed protein responsive programmable DNA assembly (PRPDA) protein detection scheme and discusses the general background on biosensors. In chapter 2, I have elaborated on the instrumentation for electrochemical measurement and sensor preparation protocols. In section 3.1 we have presented the evidence of the surface modification to prepare the sensor towards the development of the PRPDA protein detection assay. The decreasing trend of the reduction and oxidation peak current ($Bare \rightarrow Probe \rightarrow Target$) of the Cyclic voltammetry indicates the presence of the immobilized probe on the bare gold surface. Section 3.2 demonstrated the finding of the comparative study performed with different pulse voltammetry technique (DPV, SWV, ACV) to achieve the highest target signal. SWV results in the highest target signal with the shortest time required to accomplish each scan among the techniques studied.

Section 3.2 presents the experiment performed to determine the highest signal to noise ratio. It is the evidence from this analysis that, 1 μM target shows 105 times higher signal to noise ratio in buffer compared to the 1 uM signal change obtained for the FiCN system. Buffer system shows detectable signal up to 1 pM target concentration.

In section 3.4, I have demonstrated the development of the strand displacement beacon, which is an essential hybridization formation reaction in the PRPDA protein detection assay. The three-way-junction forms in the PRPDA upon binding protein to the protein-specific legend in the PRPDA system, a three-way junction forms and releases an MB modified single-stranded reporter probe, which is then detected using hybridization on the sensor prepared by immobilizing with the complementary protected capture

probe on the gold surface. Here we have simulated the hybridization detection of released reporter probe in the PRPDA. This hybridization occurs by means of strand displacement reaction. A Limit of Detection was calculated to be 10 nM of this assay with a detectable signal up to 1 pM. Along with the successful development of the strand displacement assay, this experiment also suggests that the background signal arises due to the nonspecific adsorption and unwanted hybridization, which potentially limit us to lower the LOD further.

In section 3.5, we presented the results of the optimization experiment performed to lower the background signal caused by the nonspecific adsorption of MB on gold and unwanted hybridization due to target independent TWJ formation. Following 4 experiment was conducted; These are; (1) Controlled temperature protocol for probe protection, (2) extra protection the probe on the sensor, (3) Dilution of the reporter probe, (4) With Poly A in the target solution as an additional surface blocker. The evidence from this experiment suggests that by introducing a control duplex preparation protocol and introducing poly A in the target solution the signal to noise ratio could be improved significantly.

We varied poly A concentration to find an optimum point when it provides the highest signal to noise ratio. The evidence from the experimental results suggests that by introducing 1 uM poly A it is achievable to get 4900 % signal difference for the target to control.

The subsections in section 3.5 demonstrated a time depended binding kinetics experiment to minimize the unwanted hybridization occur due to target independent TWJ formation. At 30 min target independent TWJ formation shows the highest target peak current to blank peak current ratio.

Finally, in section 3.6, we performed the PRPDA protein detection assay on the

planar and wrinkled gold electrodes. We have calculated the limit of detection to be 1 pM on the wrinkled gold electrode which is tenfold higher compare the LOD of 10 pM calculated on the planar gold electrode. This evidence fits with the objects discussed in the chapter-1.

4.3 Conclusions and Future direction

In this thesis we demonstrated that by employing electrochemical transduction technique and nonporous gold electrode it was possible to improve Limit of Detection (LOD) of 1 pM for the protein detection using PRPDS assay compared to the LOD of 2.5 nM reported with a similar assay for the protein detection utilizing fluorescence transduction technique by Li et. al. [1]. Though, the lowest detection limits achieved with our system is 1 pM on the nonporous wrinkled gold electrodes, we were able to achieve detectable signals up to 1 fM, which suggests that if the background signal were further reduced, it would be possible to push the LOD to lower than 1 pM with the same system developed in this work. In future, LOD can be lowered by exploring different surface blockers to reduce background signal produced due to nonspecific adsorption, such as polyethylene glycol (PEG) [61], Poly-C sequence [55], Succinic Anhydride (SA), Bovine Serum Albumin (BSA)[62] etc. Herein, we have demonstrated the detection of streptavidin, in future, the detection can demonstrate to actual disease marker like prostate-Prostate Specific Antigen (PSA). It was reported that presence of PSA concentration higher then 0.13 nM in the mens blood considered as cancerous [63]. Another potential work can be done by introducing this system to microfluidics devices to achieve real-time protein detection.

Bibliography

1. Li, F., Lin, Y. & Le, X. C. Binding-induced formation of DNA three-way junctions and its application to protein detection and DNA strand displacement. *Analytical chemistry* **85**, 10835–10841 (2013).

2. Schrodi, S. J. *et al.* Genetic-based prediction of disease traits: prediction is very difficult, especially about the future. *Frontiers in genetics* **5** (2014).

3. Mehrotra, P. Biosensors and their applications–A review. *Journal of oral biology and craniofacial research* **6**, 153–159 (2016).

4. Cammann, K. Bio-sensors based on ion-selective electrodes. *Fresenius' Journal of Analytical Chemistry* **287**, 1–9 (1977).

5. Thévenot, D. R., Toth, K., Durst, R. A. & Wilson, G. S. Electrochemical biosensors: recommended definitions and classification. *Biosensors and Bioelectronics* **16**, 121–131 (2001).

6. Thevenot, D. R., Toth, K., Durst, R. A. & Wilson, G. S. Electrochemical biosensors: recommended definitions and classification. *Pure and applied chemistry* **71**, 2333–2348 (1999).

7. Arnold, M. A. & Meyerhoff, M. E. Recent advances in the development and analytical applications of biosensing probes. *Critical Reviews in Analytical Chemistry* **20**, 149–196 (1988).

8. Rackus, D. G., Shamsi, M. H. & Wheeler, A. R. Electrochemistry, biosensors and microfluidics: a convergence of fields. *Chemical Society Reviews* **44**, 5320–5340 (2015).

9. Chandrasekaran, A. R. DNA Nanobiosensors: An Outlook on Signal Readout Strategies. *Journal of Nanomaterials* **2017** (2017).

10. Grieshaber, D., MacKenzie, R., Voeroes, J. & Reimhult, E. Electrochemical biosensors-sensor principles and architectures. *Sensors* **8**, 1400–1458 (2008).

11. Sin, M. L., Mach, K. E., Wong, P. K. & Liao, J. C. Advances and challenges in biosensor-based diagnosis of infectious diseases. *Expert review of molecular diagnostics* **14**, 225–244 (2014).

12. *PalmSens compact Electrochemical Biosensors* <`https://www.palmsens.com/`>.

13. Hansen, J. A., Mukhopadhyay, R., Hansen, J. Ø. & Gothelf, K. V. Femtomolar electrochemical detection of DNA targets using metal sulfide nanoparticles. *Journal of the American Chemical Society* **128**, 3860–3861 (2006).

14. Silverman, A. P. & Kool, E. T. Quenched probes for highly specific detection of cellular RNAs. *TRENDS in Biotechnology* **23**, 225–230 (2005).

15. Tyagi, S. & Kramer, F. R. Molecular beacons: probes that fluoresce upon hybridization. *Nature biotechnology* **14**, 303–308 (1996).

16. Campas, M. & Katakis, I. DNA biochip arraying, detection and amplification strategies. *TrAC Trends in Analytical Chemistry* **23**, 49–62 (2004).

17. Marras, S. A., Tyagi, S. & Kramer, F. R. Real-time assays with molecular beacons and other fluorescent nucleic acid hybridization probes. *Clinica Chimica Acta* **363**, 48–60 (2006).

18. Tyagi, S., Marras, S. A. & Kramer, F. R. Wavelength-shifting molecular beacons. *Nature biotechnology* **18** (2000).

19. Piunno, P. A., Krull, U. J., Hudson, R. H., Damha, M. J. & Cohen, H. Fiber-optic DNA sensor for fluorometric nucleic acid determination. *Analytical chemistry* **67**, 2635–2643 (1995).

20. Epstein, J. R., Biran, I. & Walt, D. R. Fluorescence-based nucleic acid detection and microarrays. *Analytica Chimica Acta* **469**, 3–36 (2002).

21. Abel, A. P., Weller, M. G., Duveneck, G. L., Ehrat, M. & Widmer, H. M. Fiber-optic evanescent wave biosensor for the detection of oligonucleotides. *Analytical Chemistry* **68**, 2905–2912 (1996).

22. Sassolas, A., Leca-Bouvier, B. D. & Blum, L. J. DNA biosensors and microarrays. *Chemical reviews* **108**, 109–139 (2008).

23. Cross, G. H. *et al.* A new quantitative optical biosensor for protein characterisation. *Biosensors and Bioelectronics* **19**, 383–390 (2003).

24. Berney, H. & Oliver, K. Dual polarization interferometry size and density characterisation of DNA immobilisation and hybridisation. *Biosensors and Bioelectronics* **21**, 618–626 (2005).

25. Cao, Y. C., Jin, R. & Mirkin, C. A. Nanoparticles with Raman spectroscopic fingerprints for DNA and RNA detection. *Science* **297**, 1536–1540 (2002).

26. Isola, N. R., Stokes, D. L. & Vo-Dinh, T. Surface-enhanced Raman gene probe for HIV detection. *Analytical chemistry* **70**, 1352–1356 (1998).

27. Vo-Dinh, T. *et al.* Surface-enhanced Raman Scattering (SERS) method and instrumentation for genomics and biomedical analysis. *Journal of Raman Spectroscopy* **30**, 785–793 (1999).

28. Umek, R. M. *et al.* Electronic detection of nucleic acids: a versatile platform for molecular diagnostics. *The Journal of Molecular Diagnostics* **3**, 74–84 (2001).

29. Suni, I. I. Impedance methods for electrochemical sensors using nanomaterials. *TrAC Trends in Analytical Chemistry* **27**, 604–611 (2008).

30. Feng, Y., Yang, T., Zhang, W., Jiang, C. & Jiao, K. Enhanced sensitivity for deoxyribonucleic acid electrochemical impedance sensor: gold nanoparticle/polyaniline nanotube membranes. *Analytica chimica acta* **616**, 144–151 (2008).

31. K'Owino, I. O. & Sadik, O. A. Impedance spectroscopy: a powerful tool for rapid biomolecular screening and cell culture monitoring. *Electroanalysis* **17**, 2101–2113 (2005).

32. Li, J. *et al.* Inlaid Multi-Walled Carbon Nanotube Nanoelectrode Arrays for Electroanalysis. *Electroanalysis* **17**, 15–27 (2005).

33. Tiwari, A. & Gong, S. Electrochemical detection of a breast cancer susceptible gene using cDNA immobilized chitosan-co-polyaniline electrode. *Talanta* **77**, 1217–1222 (2009).

34. Deng, C. *et al.* Impedimetric aptasensor with femtomolar sensitivity based on the enlargement of surface-charged gold nanoparticles. *Analytical chemistry* **81**, 739–745 (2008).

35. Soleymani, L., Fang, Z., Sargent, E. H. & Kelley, S. O. Programming the detection limits of biosensors through controlled nanostructuring. *Nature Nanotechnology* **4**, 844–848 (2009).

36. Zhang, J. *et al.* A ratiometric electrochemical biosensor for the exosomal microRNAs detection based on bipedal DNA walkers propelled by locked nucleic acid modified toehold mediate strand displacement reaction. *Biosensors and Bioelectronics* **102**, 33–40 (2018).

37. Rowe, A., White, R., Bonham, A. & Plaxco, K. Fabrication of Electrochemical-DNA Biosensors for the Reagentless Detection of Nucleic Acids. *Proteins and Small* (2011).

38. Vo-Dinh, T. & Cullum, B. Biosensors and biochips: advances in biological and medical diagnostics. *Fresenius' journal of analytical chemistry* **366**, 540–551 (2000).

39. Lequin, R. M. Enzyme immunoassay (EIA)/enzyme-linked immunosorbent assay (ELISA). *Clinical chemistry* **51**, 2415–2418 (2005).

40. Zhang, S., Garcia-D'Angeli, A., Brennan, J. P. & Huo, Q. Predicting detection limits of enzyme-linked immunosorbent assay (ELISA) and bioanalytical techniques in general. *Analyst* **139**, 439–445 (2014).

41. Vestergaard, M., Kerman, K., Tamiya, E., *et al.* An overview of label-free electrochemical protein sensors. *Sensors* **7**, 3442–3458 (2007).

42. Nelson, S. M., Ferguson, L. R. & Denny, W. A. Non-covalent ligand/DNA interactions: minor groove binding agents. *Mutation Research/Fundamental and Molecular Mechanisms of Mutagenesis* **623**, 24–40 (2007).

43. Mahshid, S. S., Camiré, S., Ricci, F. & Vallée-Bélisle, A. A highly selective electrochemical DNA-based sensor that employs steric hindrance effects to detect proteins directly in whole blood. *Journal of the American Chemical Society* **137**, 15596–15599 (2015).

44. Papadopoulou, E. *et al.* Specifically horizontally tethered DNA probes on Au surfaces allow labelled and label-free DNA detection using SERS and electrochemically driven melting. *Chemical Science* **7**, 386–393 (2016).

45. Bard, A. J., Faulkner, L. R., Leddy, J. & Zoski, C. G. *Electrochemical methods: fundamentals and applications* (wiley New York, 1980).

46. Wang, J., Luo, D. B., Farias, P. A. & Mahmoud, J. S. Adsorptive stripping voltammetry of riboflavin and other flavin analogs at the static mercury drop electrode. *Analytical chemistry* **57**, 158–162 (1985).

47. Osteryoung, J. G. & Osteryoung, R. A. Square wave voltammetry. *Analytical Chemistry* **57**, 101–110 (1985).

48. Gorodetsky, A. A., Buzzeo, M. C. & Barton, J. K. DNA-mediated electrochemistry. *Bioconjugate chemistry* **19**, 2285–2296 (2008).

49. Fang, B., Jiao, S., Li, M., Qu, Y. & Jiang, X. Label-free electrochemical detection of DNA using ferrocene-containing cationic polythiophene and PNA probes on nanogold modified electrodes. *Biosensors and Bioelectronics* **23**, 1175–1179 (2008).

50. Wang, J., Rincón, O., Polsky, R. & Dominguez, E. Electrochemical detection of DNA hybridization based on DNA-templated assembly of silver cluster. *Electrochemistry communications* **5**, 83–86 (2003).

51. Boon, E. M. *et al.* Reduction of ferricyanide by methylene blue at a DNA-modified rotating-disk electrode. *Langmuir* **19**, 9255–9259 (2003).

52. Ramaley, L. & Krause, M. S. Theory of square wave voltammetry. *Analytical Chemistry* **41**, 1362–1365 (1969).

53. Guo, Y. *et al.* Recent advances in molecular machines based on toehold-mediated strand displacement reaction. *Quantitative Biology*, 1–17 (2017).

54. Huang, Z., Liu, B. & Liu, J. Parallel Polyadenine Duplex Formation at Low pH Facilitates DNA Conjugation onto Gold Nanoparticles. *Langmuir* **32**, 11986–11992 (2016).

55. Lu, C. *et al.* Poly-cytosine DNA as a High-Affinity Ligand for Inorganic Nanomaterials. *Angewandte Chemie International Edition* **56**, 6208–6212 (2017).

56. Adams-McGavin, R. C. *et al.* Nanoporous and wrinkled electrodes enhance the sensitivity of glucose biosensors. *Electrochimica Acta* **242**, 1–9 (2017).

57. Gabardo, C. M. *et al.* Rapid prototyping of all-solution-processed multi-lengthscale electrodes using polymer-induced thin film wrinkling. *Scientific Reports* **7** (2017).

58. Daggumati, P., Matharu, Z., Wang, L. & Seker, E. Biofouling-resilient nanoporous gold electrodes for DNA sensing. *Analytical chemistry* **87**, 8618–8622 (2015).

59. Atighilorestani, M. & Brolo, A. G. Comparing the Electrochemical Response of Nanostructured Electrode Arrays. *Analytical Chemistry* **89**, 6129–6135 (2017).

60. Gabardo, C. M., Hosseini, A. & Soleymani, L. A New Wrinkle in Biosensors: Wrinkled electrodes could be a breakthrough for lab-on-a-chip devices. *IEEE Nanotechnology Magazine* **10**, 6–18 (2016).

61. Kumar, S. *et al.* PEG-labeled nucleotides and nanopore detection for single molecule DNA sequencing by synthesis. *Scientific reports* **2** (2012).

62. Taylor, S., Smith, S., Windle, B. & Guiseppi-Elie, A. Impact of surface chemistry and blocking strategies on DNA microarrays. *Nucleic Acids Research* **31**, e87–e87 (2003).

63. Barry, M. J. Prostate-specific–antigen testing for early diagnosis of prostate cancer. *New England Journal of Medicine* **344**, 1373–1377 (2001).